



## Monitoring CO<sub>2</sub> in diverse European cities: Highlighting needs and challenges through characterisation

Ida Storm<sup>1,2</sup>, Ute Karstens<sup>1</sup>, Claudio D’Onofrio<sup>1</sup>, Alex Vermeulen<sup>1</sup>, Samuel Hammer<sup>3</sup>, Ingrid Super<sup>4</sup>, Theo Glauch<sup>3,5</sup>, and Wouter Peters<sup>2,6</sup>

5 <sup>1</sup>ICOS ERIC - Carbon Portal, Department of Physical Geography and Ecosystem Sciences, Lund University, Lund, 22362, Sweden

<sup>2</sup>Environmental Sciences Group, Wageningen University, 6700 AA Wageningen, the Netherlands

<sup>3</sup>Institute of Environmental Physics, Heidelberg University, Heidelberg, 69117, Germany

<sup>4</sup>Department of Air Quality & Emissions Research, TNO, 3508 TA Utrecht, the Netherlands

10 <sup>5</sup>Institut für Physik der Atmosphäre, Deutsches Zentrum für Luft- und Raumfahrt, Oberpfaffenhofen, 82234, Germany

<sup>6</sup>Centre for Isotope Research, University of Groningen, 9747 AG Groningen, the Netherlands

*Correspondence to:* Ida Storm ([ida.storm@nateko.lu.se](mailto:ida.storm@nateko.lu.se))

**Abstract.** For the development of a joint European capacity for monitoring CO<sub>2</sub> emissions, we created the framework “CO<sub>2</sub> Monitoring Challenges City Mapbooks v1.0” (acronym CMC-CITYMAP). It includes a Jupyter notebook tool (Storm et al., 2025a, <https://doi.org/10.18160/P8SV-B99F>) which we use to characterise and cluster cities based on aspects relevant for different CO<sub>2</sub> monitoring challenges, including (a) determining background levels of CO<sub>2</sub> inflow into a city (“background challenge”), (b) separating the anthropogenic emissions from the influence of the biosphere (“biogenic challenge”), (c) representing spatially and temporally non-uniform emissions in models (“modelling challenge”), and (d) implementing observation strategies not covered by the other challenges (“application-specific observational challenge”). We provide and discuss the challenges city-by-city basis, but our primary focus is on the relationships between cities: best practices and lessons learned from monitoring CO<sub>2</sub> emissions in one city can be transferred to other cities with similar characteristics. Additionally, we identify cities with characteristics that strongly contrast with those of cities with existing urban monitoring systems.

25 While the notebook tool includes 308 cities, this paper focuses on the results for 96 cities with more than 200,000 inhabitants, with a particular emphasis on Paris, Munich, and Zurich. These cities are pilot cities for the Horizon 2020-funded project Pilot Application in Urban Landscapes (“ICOS Cities”), where a range of urban CO<sub>2</sub> monitoring methods are being implemented and assessed. According to our analyses, Zurich — and Munich especially — should be less challenging to monitor than Paris. Examining the challenges individually reveals that the most significant relative challenge is the “modelling challenge” (c) for Zurich and Paris. Complex urban topography adds to the challenge for both cities, and in Zurich, the natural topography further amplifies the challenge. Munich has low scores across all challenges, but with the greatest challenge anticipated from the “application-specific observational challenge” (d). Overall, Bratislava (Slovakia) and Copenhagen (Denmark) are among the most distant from Paris, Munich, and Zurich in our dendrogram resulting from numerical cluster-analysis. This makes them



35 strong candidates for inclusion in the ICOS Cities network, as they would potentially provide the most information on how to monitor emissions in cities that face different challenges.

## 1 Introduction

“Cities are where the climate battle will largely be won or lost,” stated United Nations Secretary-General António Guterres at the 2019 C40 Mayors Summit. Cities account for approximately 67-72% of global CO<sub>2</sub>-equivalent emissions (Lwasa et al., 2022), and this share will increase as the urban population is projected to rise from 4.2 billion in 2018 to 6.7 billion by 2050 (United Nations, 2018). In response, many cities in Europe are committed to the EU’s climate targets to achieve net-zero emissions by mid-century (European Commission, 2019). Often, they have joined forces in their efforts through initiatives such as C40 Cities (C40 Cities, n.d) and the Covenant of Mayors (Covenant of Mayors, n.d.), as well as inclusion in the European Union’s mission “100 Climate-Neutral and Smart Cities by 2030” (European Commission, Directorate-General for Research and Innovation, 2024). Cities can achieve climate neutrality by ensuring they remove as much greenhouse gases as they emit. To reach this goal, they have drawn up and committed themselves to implement climate action plans with various mitigation efforts. However, many cities lack the detailed and timely information on their emission history and trends, which is necessary to evaluate effective action (Hsu, 2020). While various options exist for obtaining this information, verifying emissions always require actual observations. Determining the most effective strategies for these observations is an active area of research.

50 Most cities that engage in emission monitoring use “bottom-up” approaches that usually do not include direct observations: activity data (such as traffic counts) are combined with emission factors (such as kgCO<sub>2</sub>/vehicle), and the sophistication of its implementation varies. Several public protocols are available for cities to develop self-reported inventories (SRIs), including those from ICLEI - Local Governments for Sustainability, and the Global Covenant of Mayors (ICLEI, n.d; Global Covenant of Mayors, 2023). The estimates resulting from using different protocols can show significant differences (e.g., Albarus et al., 2023; Gurney et al., 2021; Gately and Hutyra 2017; Lian et al., 2023). For example, Gurney et al. (2021) found an average under-reporting of 18.3%, with a range from -145.5% to +63.5% when comparing the annual emission estimates for 48 U.S. cities with local SRIs to the common inventory “Vulcan”, which is consistent with observations (Gurney et al., 2020; Lauvaux et al., 2020; Basu et al., 2020). Uncertainties become even larger when estimating emissions at higher spatial and temporal resolutions (Super et al., 2021). For example, Lian et al. (2023, Fig. S10) showed particularly large discrepancies in individual 60 1 km<sup>2</sup> grid cells when comparing two emission inventories.

In the “top-down” approach, various types of observations are used to verify and potentially refine the emission estimates. The observational methods available include—but are not limited to—measuring concentrations using sensors of varying accuracy and precision, observing total column concentrations through surface-based remote sensing and satellites, and measuring direct 65



fluxes with eddy covariance. However, these observations concern total CO<sub>2</sub>. To isolate the fossil fuel component, different types of observations should be used, including those of co-emitted trace gases such as CO (e.g. Turnbull et al., 2006; Nathan et al., 2018) and NO<sub>x</sub> (e.g. Lopez et al., 2013), co-located trace gases such as SF<sub>6</sub> (e.g. Turnbull et al., 2006; Turnbull et al., 2011), or isotopes like <sup>14</sup>C in CO<sub>2</sub> (e.g. Turnbull et al., 2006; Lopez et al., 2013; Miller et al., 2020). There are many different options for using observations to provide information on emissions, often synergistically to improve each other (Miles et al., 2021). A comprehensive account of the options can be found in IG3IS “Urban Greenhouse Gas Emission Observation and Monitoring Good Research Practice Guidelines” (World Meteorological Organization, 2022). To produce spatially explicit maps with adjusted (bottom-up) emissions, inverse modelling is commonly applied. This approach relates the observations, or the observed upwind-downwind gradients (e.g. Bréon et al., 2015, Super et al., 2017; Staufner et al., 2016), to CO<sub>2</sub> exchanges within the city using transport models. Next, the CO<sub>2</sub> emissions are optimized to fit better with the observations. There are uncertainties also in the adjusted emissions, and a study period of at least a few years may be required to confirm a trend in the emissions with high confidence (Lauvaux et al., 2020).

Several factors make monitoring CO<sub>2</sub> emissions particularly challenging and prone to uncertainties. Based on a literature review of monitoring efforts in cities, we have identified four main areas of challenges. The first is to accurately represent the variability in boundary conditions, meaning the “background” concentration of air flowing into the city (the “background challenge”). This can significantly affect the results as the increase in concentrations from city emissions is relatively small, even for large cities. For example, in Indianapolis the enhancement is only about 3 ppm according to Lauvaux et al. (2016). Simply using models to represent the background can introduce errors that are larger than this enhancement, with Lian et al. (2021) reporting differences as large as 5 ppm for background concentration for Paris between two models. In addition, this may create seasonal biases (Sargent et al., 2018). The alternative is to use observations, which comes with the challenge of selecting spatially representative locations that have limited local flux contributions and well-understood atmospheric dynamics (Sargent et al., 2018). Seemingly homogeneous land cover classified as “cropland” may require extra attention, as the associated fluxes can vary significantly due to different management practices and crop rotation cycles. For example, in Miles et al., (2021) two background towers classified as “agricultural” gave significantly different values.

A second challenge is correctly attributing the fossil fuel CO<sub>2</sub> (ffCO<sub>2</sub>) component in observed total CO<sub>2</sub> (the “biogenic challenge”). Correlated and co-emitted trace gases, as well as <sup>14</sup>C in CO<sub>2</sub>, have already been mentioned as useful observations for this purpose. These observations can be used to optimize modelled prior biogenic fluxes in addition to the anthropogenic emissions (e.g. Miller et al., 2020). Historically, biogenic flux models have been unable to resolve urban vegetation and its associated fluxes. For example, Lian et al. (2023) found that their biogenic model only resolved the two largest parks within the Île-de-France region. They were not optimizing the biogenic fluxes and instead saw large adjustments to their prior ffCO<sub>2</sub> emissions, especially during the growing seasons. One alternative strategy has been to study only the dormant season and assume biogenic exchange to be insignificant (e.g. Lauvaux et al., 2016). Recent developments, including Urban-VPRM



100 (Hardiman et al., 2017) and the flux product used in this paper, can better resolve sub-kilometre patches of vegetation. Their  
improvement stem mainly from the use of high-resolution satellite products, but they are still parametrized with rural flux data  
and assumed to function in the same way also in urban area. However, urban management practices have been shown to  
violate this assumption. For example, Smith et al. (2019) found urban trees to have growth rates up to four times compared to  
those observed in a nearby forest. A more recent study from Havu et al., 2024, describes a significant CO<sub>2</sub> uptake for the city  
105 of Helsinki. This may potentially be attributed to higher ambient CO<sub>2</sub> mole fractions, nutrient variability, and water availability  
from irrigation. However, there are also urban studies where lower CO<sub>2</sub> uptake and decreased productivity are observed due  
to factors such as pollutant loads or poor soil conditions (Roman and Scatena 2011; Ainsworth et al. 2012). Correctly  
representing these responses in biogenic flux models is especially important when the biogenic component is large compared  
to anthropogenic emissions. Many studies have reported estimates for this, with the significance varying greatly depending on  
110 the city, season, and time of the day (e.g., Turnbull et al., 2015; Gurney et al., 2017; Sargent et al., 2018; Winbourne et al.,  
2022). In studies focused on Boston by Sargent et al. (2018) and the Washington, DC/Baltimore area by Winbourne et al.  
(2022), the influence of biogenic fluxes to the city's net flux is sometimes similar to that of the anthropogenic emissions.

The third challenge is representing the urban carbon landscape in models (the “modelling challenge”). While the biogenic  
115 fluxes are discussed separately, additional challenges arise from the highly non-Gaussian variability of emissions across both  
time and space. About 50% of emissions in Europe stem from large point sources, which are required to report their emissions  
under the EU ETS (European Union Emissions Trading Scheme) and the E-PRTR (European Pollutant Release and Transfer  
Register). Although many of these facilities report hourly emissions with high accuracy, most models are unable to use facility-  
specific data, relying instead on standard temporal profiles to scale annual totals. This can introduce large uncertainties, as  
120 demonstrated in studies by Super et al. (2020; 2021). These uncertainties are further increased close point sources, where it  
becomes difficult to represent the emission plume correctly due to the well-mixed assumption in most models (Lauvaux et al.,  
2016). Furthermore, as most emissions from point sources are released from a stack, models need to incorporate realistic  
vertical profiles (Brunner et al., 2019; Maier et al., 2022). Another challenge for transport models in the urban environment is  
to accurately represent airflow, which is complicated by variable topography and tall urban structures. There are models that  
125 can do this with some accuracy (e.g. Berchet et al., 2017; Gaudet et al., 2017), but they are computationally expensive to run.  
For example, to overcome this challenge, Berchet et al. (2017) use a catalogue-based approach where a set of pre-computed  
steady-state flow and dispersion patterns is matched hourly to actual meteorological observations. These models require highly  
spatiotemporally resolved input data, including both biogenic fluxes and anthropogenic emissions.

130 The fourth challenge within the scope of this paper is the “application-specific observational challenge”. Many challenges  
associated with implementing a basic observational network— such as high precision CO<sub>2</sub> in-situ observations on tall towers,  
low- and mid-cost sensors, ground based total column FTIRs (Fourier Transform Infrared Spectroscopy), and eddy flux towers  
— are inherently intertwined with, and at least partially addressed, by the other discussed challenges. Here, we additionally



135 include the challenges associated with the use of the isotope  $^{14}\text{C}$  in  $\text{CO}_2$  and making satellite observations.  $^{14}\text{C}$  (radiocarbon),  
can be used to estimate the amount of  $\text{ffCO}_2$  in a sample. However, high costs limit the spatial and temporal coverage of  
radiocarbon observations, and therefore co-emitted species such as  $\text{CO}$  are often used to fill the gaps. Calibration with co-  
located radiocarbon observations remains necessary. A key challenge with radiocarbon observations is accounting for the  
contribution to the atmospheric signal by radiocarbon emissions from nuclear facilities (e.g. Levin et al., 2003; Graven and  
Gruber, 2011; Bozhinova et al., 2014; Maier et al., 2023). Depending on the proximity of sampling locations to nuclear  
140 facilities, unaccounted emissions were estimated to mask about 15% of  $\text{ffCO}_2$  emissions in flask samples collected at seven  
Integrated Carbon Observation System (ICOS) stations (Maier et al., 2023). Even when considered in the  $\text{ffCO}_2$  estimates,  
obtaining the appropriate temporal resolution for these emissions is difficult, which increases uncertainties in  $^{14}\text{C}$ -based  $\text{ffCO}_2$   
estimates (Maier et al., 2023).

145 Another type of observations considered within the scope the fourth challenge is column-averaged  $\text{CO}_2$  dry air mole fraction  
( $\text{XCO}_2$ ) from satellites. These observations require a clear sky for accurate overpass measurements which can significantly  
limit the number of samples collected. For example, in a synthetic study for Berlin, Kuhlmann et al. (2019) found that only  
about 50 out of 365 plumes per year could be observed for  $\text{CO}_2$  emission monitoring purposes due to unfavourable  
meteorological conditions. Furthermore, the collected samples were higher (18%) than the daily means, requiring temporal  
150 profiles to correct for this sampling bias. However, as shown in Super et al. (2020), temporal profiles come with sometimes  
large additional uncertainties. Yet another challenge with satellite observations is that only large quantities of emissions  
provide a sufficient signal-to-noise ratio in the observed  $\text{XCO}_2$  enhancement over the city. Wang et al. (2020) suggested that  
emissions larger than  $7.33 \text{ MtCO}_2 \text{ yr}^{-1}$  ( $2 \text{ MtC yr}^{-1}$ ) from a city or a power plant might be monitored from space with the  $\text{CO}_2\text{M}$   
instrument which has a planned launch in 2026.

155 In this study, we quantify the relative difficulty posed by the four challenges by relating them to information gathered from  
relevant spatial data layers. This is done using various Geographical Information Science (GIS) techniques to condense  
information from multiple data layers into 18 city metrics. These metrics represent specific characteristics of the city, which  
are then weighted based on factors that are deemed to make emission monitoring challenging. The analyses are conducted  
systematically for 96 large cities in Europe. Maps showing structures of the cities with regards to the input datasets, as well as  
160 presentation of the results are published along with the study in so-called “mapbooks”. These may be exploited by any of the  
96 individual cities covered, or in national or pan-European monitoring strategies, such as targeted with ICOS (Integrated  
Carbon Observation System), satellite missions, and Copernicus’ monitoring and verification system (MVS). The full  
framework we created is called “ $\text{CO}_2$  Monitoring Challenges City Mapbooks v1.0” (CMC-CITYMAP) and also includes an  
165 interactive Jupyter notebook that can be downloaded or run on the ICOS Jupyter service. It allows users to update the analyse  
presented in this study and explore additional available metrics.



After an overview of our study area and the selected cities (Sect. 2.1), the development of the 18 metrics is outlined: Sect. 2.2 explains our method of quantification of the metrics from the different data sources, while Sect. 2.3 connects the metrics to the four monitoring challenges. Sect. 2.4 is detailing the methodology of integration of the metrics and their analysis. The results are then presented in four sections. They begin with the characteristics of individual cities (Sect. 3.1), proceed to city comparisons (Sects. 3.2 and 3.3), and conclude with a cluster analysis focusing on the implications for a joint European urban monitoring capacity. A discussion of the results follows (Sect. 4), and the study is concluded in Sect. 6. Section 5 provides links to relevant resources for the study, including its associated Jupyter notebook tool and mapbooks.

## 175 **2 Methods**

City characteristics are derived from a set of spatial information layers. These come from different sources, are presented at various resolutions, and are analysed in different ways (see Table 1). The geographical extent of the individual cities, defined by their boundaries, are used to subset the layers. Next, statistical properties and derived indices are aggregated to comparable characteristics for the cities. In some cases, several layers are combined to arrive at the characteristics, such as to estimate the influence of biospheric activity on the cities' total carbon budgets (see Sect. 2.2.3). When applicable, the selected time period for deriving a metric is limited to the dormant season and daytime. This helps reduce the influence of the biosphere, which is why inverse modelers often use observations collected during these times. The resulting characteristics are weighted to reflect their perceived relative importance in determining the difficulty of the individual challenges before being used in further analyses.

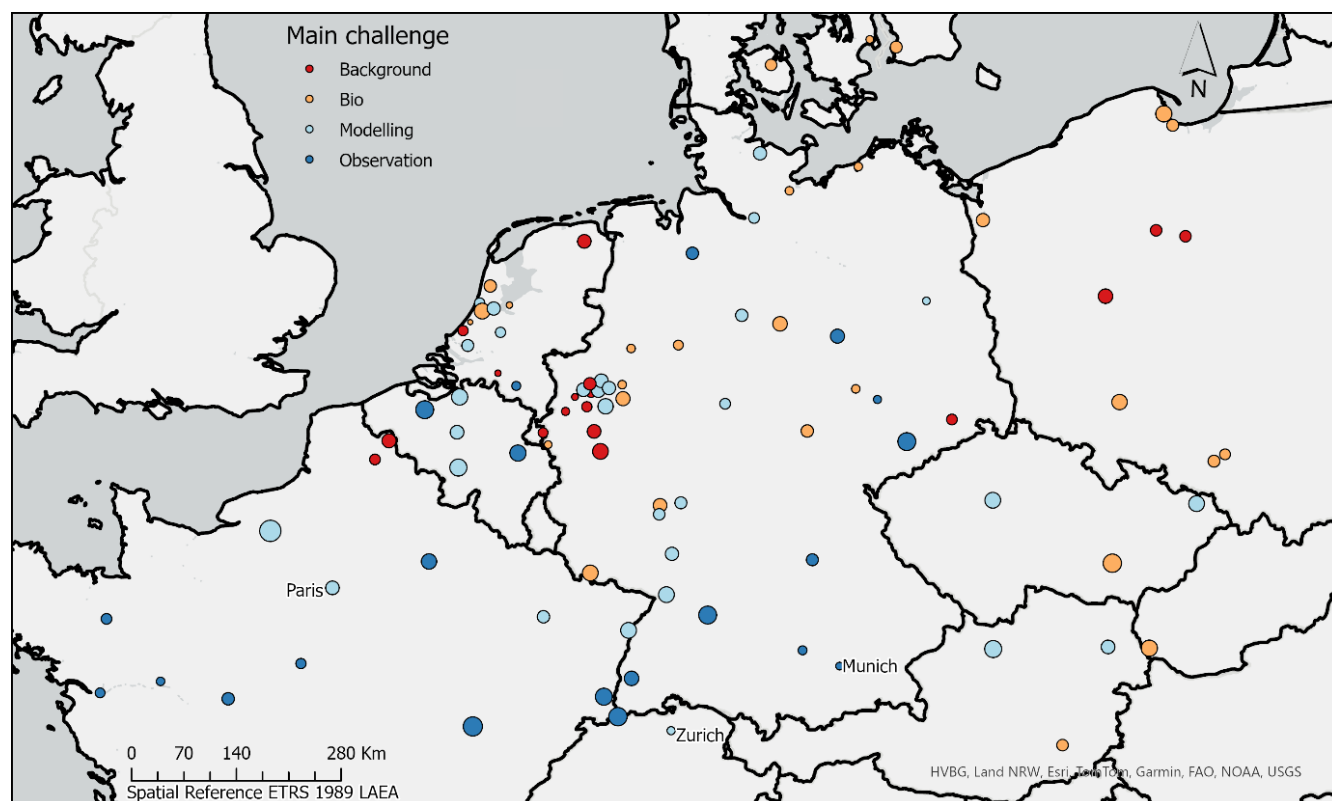
### 185 **2.1 Cities and their surroundings**

The borders representing our cities were downloaded from Eurostat's GISCO service (Eurostat, 2024). These include only cities within the European Union and the definition of a city is provided by the OECD (Organisation for Economic Co-operation and Development). Fine-grained population data was used to delineate urban centres, defined as contiguous areas of high population density (>1500 residents per km<sup>2</sup>) with a total population of at least 50,000 residents. In turn, the urban centres were associated with local administrative units, and if more than 50% of the population within a unit lived in the urban centre, the local administrative unit was defined as a city. In cases where adjacent local administrative units met the city criteria, they were merged to form a single city (Dijkstra et al., 2019).

A total of 308 cities in the European Union fall within our study region spanning from 2°W to 19°E and from 47°N to 56°N. This is the area where one of our key data sources—the high-resolution emission data from TNO (the Dutch Organization for Applied Scientific Research)—is available. TNO is looking into the computational feasibility to extend the emissions data to cover the whole of Europe. At that point, our study region may also be expanded. For our study we have considered only cities with over 200,000 residents, resulting in 96 cities depicted in Fig. 1. Most are found in Germany (43), the Netherlands (15),



France (13) and Poland (9). The surroundings of the cities are considered when deriving some of the metrics and are defined as the area extending 20 km beyond the city boundaries. Additionally, the surrounding area in the dominant 30-degree wind direction sector is used to subset data for separately weighted metrics (see Table 1; Sect. 2.2.1). This puts higher significance on the characteristics of the area upwind of the city.



205 **Figure 1: Overview of the 96 characterised cities. The points represent cities, and their colours indicate which of the four challenges has the highest score. The size of the points increases with the anticipated overall challenge to monitor emissions in them after weighing the individual challenges equally (see Sect. 2.4.1).**

## 2.2 Extraction of city characteristics

210 Table 1 lists all the input datasets along with brief information on how they are analysed to derive metrics for the cities, which are used in further analyses. Sections 2.2.1 through 2.2.6 focus on the datasets and how they are used to derive the metrics, particularly the more complex ones. Sections 2.3.1 through 2.3.4 motivate how the data layers are associated with the individual challenges to estimate their relative difficulty.

Data (section)	Resolution	Reference year data	Reference	Metric	Metric implication	Challenge (weight)
----------------	------------	---------------------	-----------	--------	--------------------	--------------------



Wind (2.2.1)	0.25° x 025°	2018	ERA5 reanalysis (Hersbach et al., 2023)	Share of wind from dominant wind direction (limited to >2 m s <sup>-1</sup> )	Expected constancy of concentration footprint	Background (30%)*
				Share of wind >2 m s <sup>-1</sup>	Stagnant flow conditions	Background (10%)*
ffCO <sub>2</sub> emissions by sector and source type (2.2.2)	1/60° x 1/120°	2018	TNO high resolution emission inventory (Kuenen et al., 2022)	Emission intensity buffer	Non-city emissions within the expected footprint	Background (20%)
				Emission intensity buffer dominant wind direction (limited to >2 m s <sup>-1</sup> )		Background (20%)
				Share point source emission		Modelling (30%)
				Non-point-source emission spatial aggregation	Expected ffCO <sub>2</sub> signal aggregation	Modelling (20%)
Land cover (2.2.3)	10m x 10m	2021	ESA Worldcover v.2 (Zanaga et al., 2022)	Vegetation heterogeneity	Expected separation of biogenic signal	Biogenic (30%)
				Share cropland in buffer	Non-city cropland within the expected footprint	Background (10%)
				Share cropland in buffer dominant wind direction (limited to >2 m s <sup>-1</sup> )		Background (10%)
Net Ecosystem Exchange (NEE) (2.2.3)	500m x 500m	2018	VPRM (Mahadevan et al., 2008; Glauch, 2024)	NEE relative to ffCO <sub>2</sub>	Signal-to-noise potential of ffCO <sub>2</sub>	Biogenic (40%)
				Average NEE		Biogenic (30%)
Building height (2.2.4)	100m x 100m	2018	GHSL: Global building heights (Pesaresi and Politis, 2023)	Average building height	Expected complexity of urban topography	Modelling (20%)
Landform (2.2.4)	90m x 90 m	2015	Global SRTM Landforms (Theobald et al., 2015)	Share of flat areas	Expected complexity of natural topography	Modelling (15%)*
Topography (2.2.4)	25m x 25m	2011	EU-DEM v1.1 (European Environment Agency, 2016)	Topographic heterogeneity		Modelling (15%)
Emissions from nuclear facilities (2.2.5)	Exact locations	2021	Annual emission totals of <sup>14</sup> CO <sub>2</sub> from nuclear facilities	Potential nuclear masking (see Eq. 1)	Expected interference of nuclear emissions when	Observational (25%)
				Nuclear sample selection bias		Observational (25%)



			(Storm et al., 2024b)		sampling radiocarbon	
Cloud cover (2.2.6)	0.25° x 025°	2018	ERA5 reanalysis (Hersbach et al., 2023)	Share of days with >30% cloud cover summer	Expected potential for satellite observations	Observational (25%)
				Share of days with >30% cloud cover winter		Observational (25%)

\* Values are inverted to make a higher value mean a greater monitoring challenge (see Sect 2.4).

215 **Table 2: An overview of the different input data layers, the metrics they are used to derive, and the specific challenges they contribute to estimating. Their weights in their contributions to the challenges are provided as percentages. For the overall challenge, the four individual challenges are equally weighted.**

### 2.2.1 Wind

For the metrics related to wind, data from European Centre for Medium-Range Weather Forecasts (ECMWF) Reanalysis v5  
 220 (ERA5; Hersbach et al., 2023) have been considered. This includes the eastward and northward wind components at 10 meters. Data during daytime hours (09:00 to 18:00 UTC) in the winter months (January and February) of 2018 was used for the analyses. One of the derived metrics is the share of times the wind speed is above  $2 \text{ m s}^{-1}$  at the centroid of the city boundary. The  $2 \text{ m s}^{-1}$  threshold is also used to filter out low wind speeds when calculating the fraction of time the wind is from the dominant wind direction.

225

The dominant wind direction is determined by aggregating the wind direction into 30-degree bins, where north is defined as ranging from 345 to 15 degrees. The bin found to represent the dominant wind direction for a city is used in several metrics, including estimating the emission intensity and share of cropland surrounding the city with an emphasize on the surrounding area in the dominant wind direction.

### 230 2.2.2 Anthropogenic CO<sub>2</sub> emissions

The bottom-up emission inventory of CO<sub>2</sub> used in this paper originates from TNO and includes emissions from different sectors distributed on a  $1/60^\circ \times 1/120^\circ$  degree grid (approx.  $1 \text{ km}^2$ ), or to their exact location in case of power plants and industrial facilities as derived from input datasets including E-PRTR (Kuenen et al., 2022, Table 1). Standard temporal profiles (updated from Denier van der Gon et al., 2011) are applied to distribute the annual emissions to hourly emissions using sector-specific scaling factors for the individual months, days of the week, and hours of the day. These profiles are used to get data  
 235 comparable to biogenic activity at specific times (see Sect. 2.2.3).

In addition to metrics related to emission intensity and shares, there is a metric called “non-point-source emission spatial aggregation”. It is defined as the share of the city’s total area with the highest emission intensity that in combination hold 50%



240 of the total emissions from non-point sources. Higher values therefore mean that remaining emissions are more evenly distributed in the city.

### 2.2.3 Biospheric CO<sub>2</sub> exchange

The biospheric CO<sub>2</sub> fluxes were provided by Heidelberg University. Their calculation of NEE (Net Ecosystem Exchange) is based on a new implementation of the Vegetation Photosynthesis and Respiration Model (VPRM; Mahadevan et al., 2008).  
245 The implementation uses the pyVPRM tool (Glauch, 2024; <https://github.com/tglauch/pyVPRM>, last access 2024-10-22). VPRM is a simple diagnostic model that uses remote sensing and meteorological data to estimate the NEE at high spatiotemporal resolution. This implementation uses MODIS Terra MOD09A1 Collection 6.1 8-day data (Vermote, E., 2021) at 500 m resolution and hourly ERA5 meteorological data with a resolution of 0.25 degrees to retrieve the two-meter temperature and the solar irradiance (Hersbach et al., 2023). Snow, cloud, and data quality cuts are applied to remove pixels  
250 that are unusable for the detection of the plant phenology. In addition, land cover information from the Copernicus Land Cover Service is used at 100m resolution (Buchhorn et al., 2020). This implementation significantly improves the vegetation detection around cities compared to older versions that used the 1-km SYNMAP vegetation map (Jung et al., 2006). VPRM model parameters have been fitted using measurements from 73 eddy covariance stations across Europe from FLUXNET (Pastorello et al., 2020) and ICOS Ecosystem data (ICOS RI, ICOS ETC, 2023) between 2012 and 2022.

255

For the metric related to the general biogenic activity in the city, average NEE at 15:00 UTC during winter (January and February) has been calculated. In the metric comparing it to the emissions, the ratio between average city-wide NEE and anthropogenic ffCO<sub>2</sub> at 15:00 UTC in winter is used. If this is a challenge during this time of year, when the biosphere is dormant, it will also be a challenge during the rest of the year. To estimate how coherent the biogenic active areas are within  
260 the city, an “edge-to-area ratio” for vegetation is applied. Based on the European Space Agency (ESA) Worldcover dataset v2 (Zanaga et al., 2022), each 10m resolution cell attributed to vegetation (classes 10, 20, 30, 40, 90, and 100) is selected. “Edge” cells, defined as having one or more neighbouring cells that are not vegetated, are identified. The final metric is the percentage of the vegetated area that is classified as edge cells.

### 2.2.4 Natural and built-up topography

265 The landform dataset by Theobald et al. (2015) is used to calculate the share of flat areas (classes 24 and 34) within the city, while average building heights are derived from the dataset by Pesaresi and Politis (2023) which is on 100x100 meter resolution. Although the coarse average building height resolution does not capture the fine-grain variability between building structures, it is adequate for a city-wide average and indicates whether the city has many tall buildings.

270 The spatial variability in the natural topography – the “spatial heterogeneity” metric – is captured by averaging the Terrain Ruggedness Index (TRI) for each 25m x 25m grid cell in the EU-DEM v1.1 (European Environment Agency, 2016). The TRI



is calculated using the methodology outlined in Riley et al. (1999): each cell's value is determined by taking the square root of the squared and averaged elevation differences with its eight adjacent cells.

### 2.2.5 Radiocarbon ( $^{14}\text{CO}_2$ )

275 When using  $^{14}\text{CO}_2$  observations to separate fossil and non-fossil contributions of urban  $\text{CO}_2$  enhancements, it is essential — particularly in Europe — to account for the impact of anthropogenic  $^{14}\text{C}$  emissions from nuclear facilities. Nuclear emissions enhance the  $^{14}\text{C}/\text{C}$  ratio masking a certain share of the  $^{14}\text{C}/\text{C}$  depletion due to the emission of  $\text{ffCO}_2$ . This masking effect is on average 15% in flask samples collected at seven ICOS stations in the study by Maier et al. (2023). We apply their methodology to estimate nuclear contributions in the 96 cities, using a Jupyter notebook hosted at the ICOS Carbon Portal (Storm et al.,  
280 2024a). To quantify nuclear masking, we use a modification of Equation 2.3 from Maier et al. (2023), where  $\text{ffCO}_2$  ( $C_{\text{ff}}$ ) is calculated using measured  $\text{CO}_2$  ( $C_{\text{meas}}$ ) and  $\Delta^{14}\text{C}$  ( $\Delta^{14}\text{C}_{\text{meas}}$ ), both with and without considering the nuclear contribution ( $\Delta^{14}\text{C}_{\text{nuc}}$ ). We exclude the relatively insignificant respiration term which was also excluded in Levin et al. (2003):

$$\Delta^{14}\text{C}_{\text{meas}} = \frac{C_{\text{bg}} \cdot \Delta^{14}\text{C}_{\text{bg}} + C_{\text{meas}} \cdot \Delta^{14}\text{C}_{\text{nuc}} - 1000 \cdot C_{\text{ff}}}{C_{\text{ff}} + C_{\text{bg}}} \quad (1)$$

285  $\Delta^{14}\text{C}_{\text{meas}}$  is solved for based on modelled concentration timeseries calculated in the Jupyter notebook (Storm et al., 2024a; Karstens, 2023). The background concentrations ( $\Delta^{14}\text{C}_{\text{bg}}$ ), however, were provided by the ICOS Radiocarbon Laboratory based on measurements from the Mace Head site in Ireland. Next, Eq. 1 is used once more to back-calculate what  $\text{ffCO}_2$  ( $C_{\text{ff}}$ ) would need to be if the nuclear contribution term ( $\Delta^{14}\text{C}_{\text{nuc}}$ ) was not considered. The result is compared to the original modelled  $\text{ffCO}_2$   
290 component ( $C_{\text{ff}}$ ) to calculate the impact of nuclear masking. For the calculation of the final metric for each city, the average differences in percent for January and February at 12:00 and 15:00 UTC is calculated.

Even when nuclear contributions are accounted for, they introduce additional uncertainties to the  $^{14}\text{C}$ -based  $\text{ffCO}_2$  estimates. These uncertainties arise primarily because the flat emission time profile, derived from the annual nuclear emissions totals,  
295 does not accurately reflect the timing of emissions (Maier et al., 2023). This is one of the motivations behind the current sampling strategy at the ICOS Radiocarbon Laboratory in Heidelberg: to avoid sampling when nuclear contribution exceeds 0.5 permil. A second metric, "nuclear sample selection bias," calculates the extent of sampling bias that could occur in cities if this strategy is adopted. The modelled concentration timeseries (12:00 and 15:00 UTC, January and February of 2021) is subset to when the nuclear contribution is below 0.5 permil, according to the calculations in the Carbon Portal notebook (Storm  
300 et al., 2024a). The average of the  $\text{ffCO}_2$  components in the subset is compared to the average  $\text{ffCO}_2$  components for the whole timeseries, resulting in a difference in percent, which is our metric.



## 2.2.6 Cloud cover

Total cloud cover is extracted from ECMWF ERA5 at 12:00 UTC during the winter (January and February) and summer (June and July) of year 2018 and are considered as separate metrics. Both summer and winter are included because cloud cover can exhibit significant seasonal differences depending on the city's location. 12:00 UTC was selected to match with the overpass time of the planned CO2M satellite mission (Kuhlmann et al., 2019). The 0.25 x 0.25 degree ERA5 data cell in which each city falls is used to extract a time series of cloud cover in the individual cities. In turn, a threshold of 30% cloud cover is used to calculate the proportion of days when samples will likely need to be discarded.

## 2.3 Monitoring challenges

### 310 2.3.1 Background challenge

The challenge of determining the background concentration of CO<sub>2</sub> upwind of the city combines wind data with both natural fluxes and anthropogenic emissions. Higher wind speeds result in larger influence regions (“footprints”), which reduce the impact of strong local sources that could interfere with the goal of obtaining spatially representative observations. This leads to generally better agreement between modeled and observed values and is one reason for excluding low-wind-speed observations from further analyses, such as in the inverse modeling studies over Paris by Bréon et al. (2015) (>2 m s<sup>-1</sup>) and Lian et al. (2023) (>3 m s<sup>-1</sup>).

Wind direction is also relevant for obtaining spatially representative measurements, as fluxes in the dominant wind direction contribute most to the signal. Even at higher wind speeds, significant influence from large point sources or an especially active biosphere can still occur. To account for this, the emission intensity and the share of cropland surrounding the city are considered, with extra weight given to the area in the dominant wind direction. Cropland is singled out because of the added difficulty in correctly representing associated fluxes, which are influenced by crop cycles and management practices. A final consideration is that when the wind predominantly comes from a single direction, fewer background towers are needed to provide suitable upwind values for most observations. This makes the city less challenging to monitor.

### 325 2.3.2 Biospheric challenge

The carbon landscape of cities includes the natural exchange of CO<sub>2</sub> through soils and the biosphere. Understanding the spatial and temporal distributions of these exchanges is necessary to isolate contribution of anthropogenic emissions from the observed CO<sub>2</sub>. To estimate how challenging this might be, the natural and anthropogenic fluxes as well as land cover are considered. Whereas models can be used to estimate the signal from the biosphere, these are associated with large uncertainties — especially in urban environments. Therefore, strong biospheric activity in the city is expected to add to this challenge. Further adding to the challenge is when the signal from the biosphere is large in comparison to that from the anthropogenic emissions, which decreases the signal-to-noise ratio (e.g. Sargent et al., 2018; Winbourne et al., 2022). If the city-wide biogenic signal is



335 coming from a coherent area, for example a large park, the challenge is reduced. In such cases, partitioning the observations is expected to be easier. This is mainly relevant when observing direct fluxes in a city, as the influence areas (“footprints”) are much smaller compared to influence areas of concentration measurements (Kljun et al., 2015).

### 2.3.3 Modelling challenge

340 For the challenge of modeling CO<sub>2</sub> exchange within the city, both anthropogenic emissions and the city's natural and urban topography are considered. Point sources add complexity to this challenge. These sources emit large quantities of CO<sub>2</sub> from high stacks and require high-resolution spatiotemporal data and models. Maier et al. (2022) demonstrated that resolving emissions from stacks, as opposed to ground-level sources, is important even in regional-scale modeling within 50 km of the emission source. Furthermore, large shares of emissions from point sources can obscure more distributed sources, making these harder to monitor. The distribution of remaining non-point source emissions is also relevant to the modelling challenge. Spatially concentrated emissions are generally easier to monitor because they limit the spatial scope of the monitoring network and increase the likelihood of detecting large emission signals. Larger emission signals improve the signal-to-noise ratio and extend the time before a monitoring network may detect the planned future decreasing signals from emissions (Albarus et al., 2024).

When it comes to the natural and urban topography, high shares of flat, uniform topography and low buildings reduce airflow complexity, which makes it easier to model the atmospheric transport.

### 350 2.3.4 Observational challenge

The metrics in this challenge relate to specific observational methods that are not covered in the other challenges: using radiocarbon to distinguish between fossil fuel and biogenic components and using satellites to make XCO<sub>2</sub> observations. As mentioned in the introduction, there are additional observational methods and these may be preferred especially if the two discussed here prove challenging (World Meteorological Organization, 2022). A well-established issue in using radiocarbon to infer ffCO<sub>2</sub> is radiocarbon emissions from nuclear facilities. "Potential nuclear masking" refers to the underestimation in ffCO<sub>2</sub> signal the nuclear contribution is modelled to cause if ignored. It is called "potential" because it can be corrected for, but large uncertainties in the correction arise from the quality of emission data and uncertain transport modelling. Hence, the challenge increases with large potential nuclear masking. A preferred practice is to avoid sampling when nuclear contribution is expected to be significant. However, this can lead to sampling bias which is estimated for the "nuclear sample selection bias" metric. Ideally, the ffCO<sub>2</sub> signal should be of similar magnitude in both avoided and collected samples. A greater difference means a greater sampling bias and adds to the observational challenge.



The metrics related to making observations using satellites is based on cloud cover. Summer and winter are considered as separate metrics as there can be large differences in cloud cover between the seasons. Higher shares of cloud cover will limit the samples from future satellite missions, thereby adding to the observational challenge.

## 2.4 Integration and analysis of city characteristics

The collected characteristics for the 96 cities are further analysed using statistical methods. These methods include the calculation of challenge scores for the individual challenges and an overall challenge score, along with associated similarity matrices. In turn, the similarity matrices facilitate similarity searches and cluster analyses. To prepare the collection to be combined, the selected characteristics are transformed using a min-max normalization between the 10-90 percentile (Eq. 2). The 10-90 percentile range is used to focus the analyses on the normal characteristic range of cities.

The scaled value of characteristic  $j$  for city  $i$  ( $x_{ij}^{scaled}$ ) is calculated as:

$$x_{ij}^{scaled} = \max(0, \min(1, \frac{x_{ij} - q_{0,1}^j}{q_{0,9}^j - q_{0,1}^j})) \quad (2)$$

Where  $q_{0,1}^j$  and  $q_{0,9}^j$  represent the 10<sup>th</sup> and 90<sup>th</sup> percentiles of the  $x_{ij}$  values across all 96 cities. The min and max functions enforce a normalized range between 0 and 1.

In most cases, a higher value of a metric can be interpreted as more challenging to monitor. However, the opposite is true for the metrics “Share of wind from dominant wind direction”, “Share of wind >2 m s<sup>-1</sup>”, and “Share of flat areas”. Therefore, resulting  $x_{ij}^{scaled}$  are inverted — meaning a value of 0 becomes a value of 1 — to ensure consistency and allow for combination of metrics into scores for the different challenges.

### 2.4.1 Challenge scores

The scaled characteristics are combined to create individual and overall challenge scores. Before they are summarized, the weights listed in Table 1—assigned based on expert knowledge and consideration of our literature review—are applied to reflect each metric’s relative importance. This means the final scores are normalized to a range between 0 and 1, or 0 and 100%, for minimum and maximum relative challenge. The minimum and maximum values can be achieved if a city consistently falls within the bottom 10<sup>th</sup> or top 90<sup>th</sup> percentile for all metrics. For the overall challenge score, which considers all metrics, the weights in Table 1 associated with the four individual challenges are divided by four before being summarized.



## 2.4.2 Similarity matrices

The scaled and weighted characteristics are used to create similarity matrices based on Euclidean distances. The Euclidean distance,  $D$ , between two cities  $x$  and  $y$  is calculated as follows:

$$395 \quad D(x, y) = \sqrt{\sum_{i=1}^n (x_i - y_i)^2} \quad (3)$$

Where  $x_i$  and  $y_i$  represent the  $i$ th scaled and weighted characteristic vectors of for cities  $x$  and  $y$  respectively.

Similarity matrices created using Euclidean distances are suitable for further analyses, including hierarchical clustering, discussed next.

## 400 2.4.3 Dendrogram cluster analysis

Based on the similarity matrix given all available metrics (see Sect 2.4.2), a dendrogram is constructed. A dendrogram is a tree-like diagram that visually represents hierarchical clusters. It starts with each city represented as an individual branch. These branches are incrementally merged according to their similarity. There are different strategies for the merging, and we used one referred to as “Ward’s method” where the total within-cluster sum of squared Euclidean distances is minimized:

$$405 \quad \Delta SS(C_i, C_j) = \frac{|C_i| \cdot |C_j|}{|C_i| + |C_j|} \cdot D(\bar{x}_i, \bar{x}_j)^2 \quad (4)$$

Where  $\Delta SS$  is the increase in the total within-cluster sum of squared distances, calculated for all possible combinations of two clusters,  $C_i$  and  $C_j$ , that can be merged.  $|C_i|$  and  $|C_j|$  represent the number of cities within each cluster.  $\bar{x}_i$  and  $\bar{x}_j$  are the  
410 centroids of these clusters. The Euclidean distances between the centroids are calculated using Eq. 3.

As clusters are merged, the dendrogram moves towards forming a single branch (see Fig. 4). The later that two branches are merged, the more dissimilar the cities in the two branches are. Before merging, the branches can be viewed as individual clusters. Visual inspection of the dendrogram tree reveals five meaningful clusters, discussed further in the result section.

## 415 3 Results

The results begin with a section that highlights some of the individual characteristics of the cities and exemplifies what several of the input spatial data layers look like (see Fig. 2). Next, the challenge scores estimated from the combination of metrics are showcased, followed by their application in similarity searches. Finally, general similarities and dissimilarities among all cities are identified based on the cluster analysis result. There is a general focus on Paris, Munich, and Zurich as these are part of the  
420 evolving urban observation network within ICOS (<https://www.icos-cp.eu/projects/icos-cities>, last access: October 2024).



Similarity searches are employed to identify the potential for knowledge exchange between cities that face similar challenges to those within the network. Finally, the cluster analysis is used to identify cities that are dissimilar to those already in the network. These cities are argued as good candidates for additions to the ICOS Cities network. More details about other specific cities can be found in the resources published along with this study (see Sect. 5).

### 425 3.1 General characteristics

The 96 selected cities exhibit a wide range of values across the different characteristics with the 90<sup>th</sup> percentile values frequently being several times higher than the 10<sup>th</sup> percentile values (see Table 2). The span of 10<sup>th</sup> to 90<sup>th</sup> percentile ranges is the most extreme for metrics where emissions from point sources are part of the analysis: while many cities have none, some have large emitters that account for almost all the emissions in the city. The non-Gaussian distribution of large emission sources also contributes to a large variability of emission intensity in the surroundings of the cities, and partly also to major differences in ratio between NEE and anthropogenic CO<sub>2</sub>. Nuclear facilities are also unevenly distributed, with particularly large amounts of radiocarbon emitted from La Hague, located on the coast of Normandy, France. This creates significant “nuclear masking potential” in a handful of cities and results in a mean value that is as large as the 90<sup>th</sup> percentile. There are also significant differences in the sampling bias introduced by adopting the strategy of discarding samples with large nuclear contribution (“representation bias sample selection”): for the 90<sup>th</sup> percentile city, the modelled average fossil fuel enhancement is very different compared to the enhancement in the discarded (38%). This broadness of characteristics poses a range of very different challenges when it comes to emission monitoring in different cities, which confirms the primary motivation for this study.

Metric	Unit	Mean	10 <sup>th</sup> percentile	90 <sup>th</sup> percentile	Std.
Share of wind >2 m s <sup>-1</sup>	%	84	73	93	10
Share of wind from dominant wind direction (limited to >2 m s <sup>-1</sup> )	%	26	21	32	5
Emission intensity buffer	tCO <sub>2</sub> km <sup>-2</sup>	5264	750	14621	6899
Emission intensity buffer dominant wind direction (limited to >2 m s <sup>-1</sup> )	tCO <sub>2</sub> km <sup>-2</sup>	5342	368	14994	12051
Share of point source emission	%	29	0	76	28
Non-point-source emission spatial aggregation	%	19	12	25	5
Vegetation heterogeneity	%	24	14	34	7
Share cropland buffer	%	30	12	51	14
Share cropland buffer dominant wind direction (limited to >2 m s <sup>-1</sup> )	%	30	5	57	21
NEE relative to emissions	%	25	8	44	22



Average NEE	$\mu\text{mol m}^{-2} \text{s}^{-1}$	0.60	0.39	0.81	0.18
Average building height	m	7.2	5.5	8.9	1.2
Share flat areas	%	44	12	71	22
Topographic heterogeneity	m	2.6	1.1	5.1	1.8
Nuclear masking potential	%	20	4.6	19.7	108
Nuclear sample selection bias	%	19	3.9	38	12
Share days >30% clouds summer	%	74	68	82	5.9
Share days >30% clouds winter	%	88	81	95	5.6

440 **Table 2: Averages, standard deviations, and 10<sup>th</sup> and 90<sup>th</sup> percentile values for the 18 metrics based on the 96 analysed cities.**

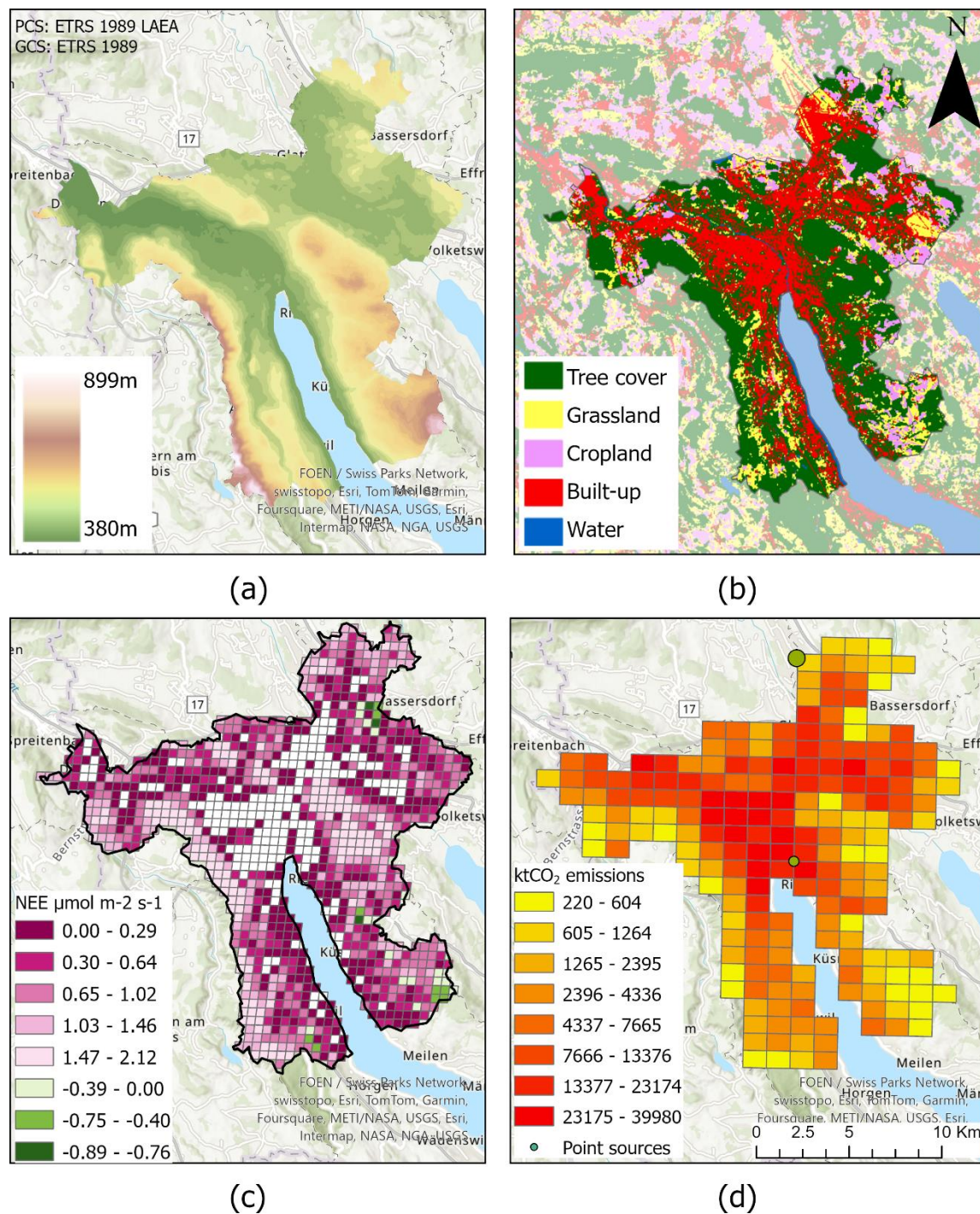


**Figure 2: Four of the input data layers subset for Zurich, showing (a) natural topography, (b) land cover, (c) biosphere net ecosystem exchange (NEE), and (d) total  $\text{ffCO}_2$ . The largest green point in the  $\text{CO}_2$  emission map (d) represents Zurich's airport and falls just outside the city border. The biogenic flux map (c) is based on an average from wintertime afternoons in 2018 (see Sect. 2.2.3).**



445 Paris stands out for its relatively low citywide NEE compared to its large ffCO<sub>2</sub> emissions which generally increase the signal-  
to-noise ratio in ffCO<sub>2</sub> emission estimates. This is seen in Fig. 3, which shows the 18 characteristics for the ICOS Cities pilot  
cities Munich, Zurich, and Paris. NEE in Paris is associated with vegetation that is fragmented, as indicated by the high  
vegetation heterogeneity metric. One implication is that this potentially makes it hard to find good locations to make eddy  
covariance measurements with limited influence of the urban biosphere. Finally, the average building height of 8.9 meters is  
450 in the 90<sup>th</sup> percentile and indicates a complex urban topography influencing the transport modelling of fluxes.

Munich and Zurich both have strong dominant wind directions which is advantageous for representing the inflow boundary  
conditions with a limited network of tall tower stations measuring concentrations. However, compared to the other cities the  
wind speed is quite frequently below 2 m s<sup>-1</sup>, which could be a challenge for collecting spatially representative up-wind  
455 observations. Both cities have low shares of emissions from point sources and are not expected to have a major problem with  
nuclear contribution in potential radiocarbon samples. Figure 2d shows the point sources in Zurich, but we note that the largest  
point source—Zurich’s airport—lies just outside the city boundaries and is therefore not included in the metric. Airports cannot  
be represented with take-off and landing information in the TNO emission inventory and are therefore rather turned into point  
sources which keeps their exact location.

460

All three cities differ significantly when it comes to natural topography; Zurich stands out with only 6% flat areas and a high  
topographic variability, placing it in the 90<sup>th</sup> percentile in both these metrics (see Fig. 2a). Similar to the complex urban  
topography in Paris, this will make modelling in Zurich particularly challenging. Out of the three cities, Munich has the most  
advantageous natural and urban topography for monitoring ffCO<sub>2</sub> emissions.



465

**Figure 3: (a) The 18 metrics listed along the y-axis are linearly scaled between the values of the city at the 10<sup>th</sup> percentile and the city at the 90<sup>th</sup> percentile, out of the 96 cities (see Table 2). They are organized along the y-axis according to their association with the four discussed challenges. Higher values indicate greater challenges to monitor CO<sub>2</sub> emissions. (b) Density plot showing where most cities fall in the linear scaling between the 10<sup>th</sup> and 90<sup>th</sup> percentile.**



### 470 3.2 Challenge scores

The combined challenge scores (see Sect. 2.4.1) range from 30% for Leiden, the Netherlands—indicating relatively low challenge—to 59% for Rouen, France as seen in Table 3. The biogenic and modelling challenges contribute the most to these scores for the two cities, respectively. There are no apparent spatial patterns regarding which challenge is estimated to have the highest scores for the cities, except in and around the Ruhr area in western Germany (see Fig. 1). Here, many cities can expect it to be challenging to determine background concentrations. A main driver is that many of these cities are close to each other, resulting in high emission intensity in their surroundings.

Among the three target cities, Munich has a low overall challenge score (34%) close to that of Leiden. Compared to other cities, the scores associated with the biogenic challenge and modelling challenges are particularly low (see Table 3). Like for Paris, the ratio between NEE and ffCO<sub>2</sub> emission is small, and for Munich the average NEE is also relatively low placing the city in the 10<sup>th</sup> percentile of the biospheric challenge (see Fig.3). While Zurich’s overall score is similar to Munich’s, the individual challenges are different, in particular for the modelling challenge where the city’s complex urban and natural topography stand out. Paris has the highest overall score of the three and stands out for its high score in the challenge of determining background concentrations. Paris is also in the third quartile when it comes to the observational and modelling challenges. Contributing factors include a high concentration of emissions from point sources and tall buildings, as well as high cloud cover especially in the summer, which likely reduces the number of useful satellite observations. The influence of nuclear emissions is the highest among the three pilot cities, but remains relatively low compared to all 96 cities considered.

City	Overall		Background		Biogenic		Modelling		Observational	
	%	Q and R*	%	Q and R*	%	Q and R*	%	Q and R*	%	Q and R*
Munich, DE	34	Q1 (6)	31	Q2 (25)	30	Q1 (9)	26	Q1 (17)	50	Q3 (65)
Zurich, CH	35	Q1 (9)	20	Q1 (5)	34	Q1 (19)	54	Q3 (70)	32	Q2 (26)
Paris, FR	45	Q3 (65)	45	Q3 (61)	38	Q2 (29)	50	Q3 (57)	48	Q3 (61)
Leiden, NL	<b>30</b>	<b>Q1 (1)</b>	32	Q2 (30)	33	Q1 (17)	30	Q2 (26)	24	Q1 (16)
Rouen, FR	<b>59</b>	<b>Q4 (96)</b>	38	Q2 (41)	41	Q2 (35)	80	Q4 (96)	76	Q4 (92)
Kassel, DE	40	Q2 (34)	<b>14</b>	<b>Q1 (1)</b>	50	Q3 (66)	56	Q4 (76)	41	Q2 (41)
Groningen, NL	45	Q3 (49)	<b>70</b>	<b>Q4 (96)</b>	66	Q4 (85)	9	Q1 (5)	38	Q2 (28)
Rennes, FR	40	Q2 (29)	42	Q3 (58)	<b>18</b>	<b>Q1 (1)</b>	40	Q2 (40)	57	Q4 (80)
Gliwice, PL	42	Q2 (45)	27	Q1 (17)	<b>76</b>	<b>Q4 (96)</b>	18	Q1 (6)	47	Q3 (57)
Almere, NL	32	Q1 (3)	39	Q2 (46)	49	Q3 (61)	<b>1</b>	<b>Q1 (1)</b>	39	Q2 (38)
Rouen, FR	59	Q4 (96)	38	Q2 (41)	41	Q2 (35)	<b>80</b>	<b>Q4 (96)</b>	76	Q4 (92)



Düsseldorf, DE	39	Q2 (28)	64	Q4 (94)	39	Q2 (31)	51	Q3 (62)	<b>0.</b>	<b>Q1 (1)</b>
									<b>3</b>	
Dijon, FR	55	Q4 (95)	36	Q2 (36)	38	Q2 (28)	53	Q3 (69)	<b>93</b>	<b>Q4 (96)</b>

\* “Q & R” stands for *Quartile and Rank*.

490 **Table 3: Challenge scores for Paris, Munich, and Zurich along with the cities with the highest and lowest scores overall, and for each of the four challenges. The higher the score, the greater the anticipated challenge.**

### 3.3 Similarity searches

Similarity matrices quantify the potential to transfer the CO<sub>2</sub> monitoring experience gained in the three ICOS pilot cities, as exemplified for Munich. The potential is especially high for cities with high similarity scores to Munich, as listed in the first section of Table 4. Strategies used to overcome the challenge of determining background concentrations in Munich could also work in Linz (Austria), Mulhouse (France), and Augsburg (Germany). These are cities where, as in Munich, this challenge is relatively low (see Table 3). In practice, this could mean that only a few background towers are needed in the outskirts of the cities to get representative boundary conditions for most situations. The biogenic challenge in Munich is also low, as in similar cities including Brussels (Belgium), Nantes, and Lille (France). It will not be as difficult to separate the anthropogenic signal in these cities as it is in cities at the opposite end of the spectrum from Munich, such as Bratislava (Slovakia) and Erfurt and Hagen (Germany), which are listed as the most dissimilar to Munich in this aspect (see Table 4).

Out of the 96 cities, Nuremberg is overall the city most like Munich, while the corresponding cities for Zurich and Paris are German cities Kassel and Berlin. Their monitoring strategies could look similar, but to overcome individual challenges it may still be useful to consider similarities in terms of the specific challenges. In terms of background challenges, Karlsruhe (Germany) is most like Zurich, and Charleroi (Belgium) to Paris. Charleroi is also most similar to Paris regarding biogenic challenges, and for Zurich, the corresponding city is Brussels (Belgium). Tables showing the top five similar cities to each of the 96 cities across the different challenges are available in the map books (see Sect. 5).

Overall (%)	Background (%)	Biogenic (%)	Modelling (%)	Observational (%)
<b>Most similar</b>				
Nuremberg, DE (92)	Linz, AT (98)	Brussels, BE (100)	Tilburg, NL (97)	Graz, AT (97)
Vienna, AT (92)	Mulhouse, FR (98)	Nantes, FR (100)	Angers, FR (96)	Vienna, AT (97)
Augsburg, DE (91)	Augsburg, DE (96)	Lille, FR (100)	Orléans, FR (96)	Bratislava, SK (95)
Hanover, DE (91)	Ostrava, CZ (95)	The Hague, NL (100)	Lens, FR (96)	Gliwice, PL (94)
Paris, FR (91)	Zurich, CH (93)	Antwerp, NL (100)	Mönchengladbach, DE (95)	Wrocław, PL (92)



Most dissimilar				
Haarlemmermeer, NL (80)	Haarlemmermeer, NL (62)	Bratislava, SK (42)	Antwerp, NL (66)	Nates, FR (56)
Gdynia, PL (80)	Groningen, NL (63)	Erfurt, DE (42)	Karlsruhe, DE (67)	Rennes, FR (56)
Odense, DE (81)	Cologne, DE (64)	Hagen, DE (42)	Gelsenkirchen, DE (67)	Lens, FR (57)
Groningen, NL (81)	The Hague, NL (65)	Münster, DE (42)	Linz, AT (67)	Angers, FR (59)
Alkmaar, NL (81)	Rotterdam, NL (65)	Saarbrücken, DE (42)	Mannheim, DE (68)	Reims, FR (59)

510

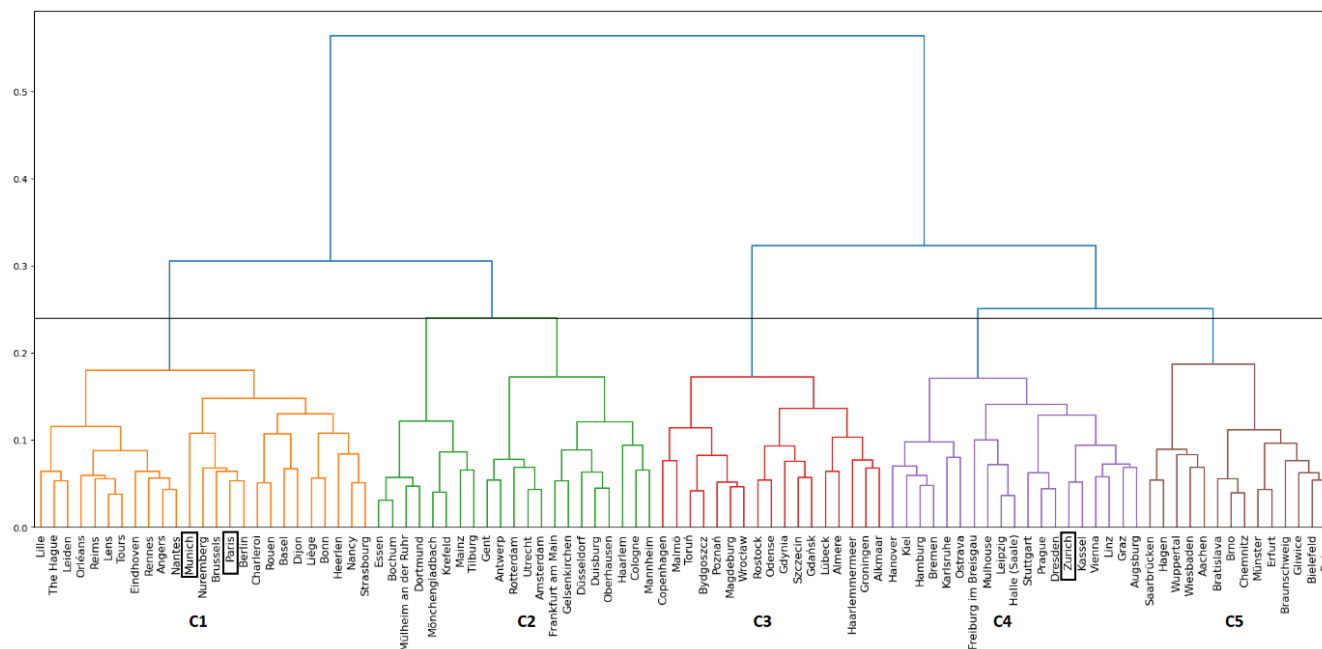
**Table 4: Similarity to Munich in terms of the four individual challenges, as well as overall similarity when the four challenges are combined. A higher value indicates greater similarity.**

### 3.4 Cluster analysis

As a complement to the similarity searches, the result from a dendrogram cluster analysis shows the overall structure of similarities and dissimilarities across all 18 metrics (see Fig. 4). The matching of cities with the ICOS Cities pilot cities, as exemplified in Sect. 3.3, would improve for many of the 96 cities more clusters were represented by pilot cities. Hence, the dendrogram can be used to guide future network expansion. Munich and Paris both fall into the same cluster, C1, whereas Zurich is in cluster C4 (see Fig. 4). The hierarchical structure of the dendrogram shows that cities in cluster C3, followed by those in cluster C5, are the furthest away in the cluster space from the already represented clusters. A prominent city in cluster C3 is Copenhagen, Denmark. Its characteristics signature (see CMC-CITYMAP; Sect. 5) indicate that Copenhagen is expected to face a greater biogenic challenge compared to the pilot cities. Using complementary observations of correlate trace gases or isotopes to separate the ffCO<sub>2</sub> signal will be especially important in these cities. However, the use of  $\Delta^{14}\text{C}$  would come with the additional uncertainty of accounting for nuclear emissions which has a significant influence in Copenhagen. This aspect of the city adds to its observational challenge. Both the background and the modelling challenges are relatively minor; the greatest challenges stem from the lack of a dominant wind direction and the average building height, which is high—though not as high as in Zurich and Paris.

Bratislava, Slovakia, is a good candidate from cluster C5 and faces an even higher biogenic challenge than Copenhagen. However, the vegetation is relatively clustered in space which offers greater opportunity to make observations where the biogenic influence is limited. Bratislava also stands out for its high share of cropland surrounding the city, which complicates determination of representative background levels of CO<sub>2</sub>. A solution could be to have more background sites to capture the potential cropland flux heterogeneity. Cities in the final cluster, C2, are closer in the cluster space to cities in clusters that already have pilot cities (see Fig. 4) but could be prioritized next.

530



535

**Figure 4: Dendrogram based on the similarity matrix created from all 18 metrics. The different colours represent five distinct clusters formed by drawing a horizontal line at the desired separation between the dendrogram branches. Paris (C1), Munich (C1), and Zurich (C4) are highlighted on the x-axis.**

#### 4 Discussion

540 Our study is sensitive to the selection of cities included in the analysis, and our focus is on a subregion in western Europe (see Fig. 1). If cities from a broader geographic area, spanning different climate zones, were included, the value ranges would likely change. For example, we would expect a wider range in the cloud cover metric, as some regions experience consistent cloudy conditions for part of the year. Large point sources in additional cities could raise the already high 90<sup>th</sup> percentile values in related metrics. For example, 13 out of our 96 cities account for 75% of the point source emissions. This results in the skewed  
 545 distribution seen in Fig. 3b, where a city like Paris—with 19% of emissions from point sources—receives a score of only 0.25 out of 1, with 1 indicating the highest level of challenge.

Another important aspect affecting the results is how our cities are defined geographically. Our city borders are based on the OECD definition of a city (Dijkstra et al., 2019), but these still rely on local administrative boundaries provided by the  
 550 countries. Albarus et al. (2023) observe that the drawing of administrative boundaries sometimes results in cities being separated from large portions of emissions in their immediate surroundings. At other times, the boundaries may include extended areas of nonurban land cover. The former scenario places greater demands on CO<sub>2</sub> emission monitoring to distinguish between emissions within and outside the borders (Albarus et al., 2023). This issue is partly addressed in our study as adjacent administrative units with high population densities form a single city (Dijkstra et al., 2019). However, significant nearby



555 emission sources may still be excluded, as seen in Zurich, where its airport falls just outside the city boundaries (see Fig. 2d).  
One option could be to consider emission intensity, rather than population, as a criterion for merging local administrative units  
in the OECD approach. This would preserve the advantage of integrating readily available statistics from local administrative  
units in future analyses. Another alternative could be to define city boundaries entirely based on the highest-resolution emission  
560 areas on the outskirts of cities, which particularly affects our urban vegetation-related metrics. For example, in Münster  
(Germany), 85% of the city area is covered by vegetation, and it was modelled to be a net source of CO<sub>2</sub> equivalent to 48% of  
that from anthropogenic emissions during the winter afternoons.

Our selection of metrics and their synthesis into four challenges is motivated by our review of literature covering emission  
565 monitoring efforts in cities. Some of these studies present results that can be discussed in the context of our findings. Previous  
studies in Paris shed light on what we refer to as the “background challenge”, where Paris scores in the 3<sup>rd</sup> quartile. The  
relatively high score for Paris aligns with the findings of Sargent et al. (2018), who warned that boundary conditions can be  
particularly complex for continental cities due to long- and medium-range transport from both distant urban areas and biogenic  
sources. Lian et al. (2021) indeed found especially large discrepancies between different modelled boundary conditions when  
570 air was coming from continental Europe—up to 5 ppm between two products. This is significant, as the CO<sub>2</sub> gradients between  
urban and suburban “background” towers in Paris were found to be 5-10 ppm in the summer and 20-30 ppm in the winter  
(Lian et al., 2023). In cities or regions with lower emission intensities than Paris, a bias in the boundary conditions would be  
even more impactful. For example, Lauvaux et al. (2012) found that a 0.55 ppm bias in the boundary condition resulted in a  
substantial impact on the posterior annual CO<sub>2</sub> flux for Iowa and the surrounding states.

575 Best practices proposed to mitigate the background challenge include using observations to find upwind-downwind gradients  
for inversions (e.g., Bréon et al., 2015; Stauffer et al., 2016) or to constrain the modelled boundary conditions with observations  
(e.g., Sargent et al., 2018). Our metrics associated with the challenge offer an estimate for how spatially representative the  
observations may be by considering fluxes nearby the cities. Our consideration of wind speed and direction also ties to how  
580 many useful observations would be available for the different practices to limit the bias from boundary conditions: these  
aspects greatly reduced the number of samples that could be used in the inversion over Paris by Bréon et al. (2015). At the  
time, the background concentration was sampled from only two towers, and the wind speed threshold, like ours, was 2 m s<sup>-1</sup>.

Regarding the “biogenic challenge”, Lian et al. (2023) highlighted their poorly resolved and non-optimized biogenic fluxes as  
585 a key area for improvement in future studies in Paris. It was pointed out as a likely contribution to the 20% increase in their  
optimized ffCO<sub>2</sub> estimates compared to the emission inventory used as prior (April-June). Different borders for Paris (Lian et  
al., 2023; Fig. 1) are just one of the reasons we cannot directly compare our results, but based on our analysis the significance  
of the biosphere is not surprising: even in the winter afternoons the modelled net influence of the biosphere is 8% compared



to the ffCO<sub>2</sub> emissions, and on summer afternoons the NEE is more than twice the magnitude of the anthropogenic emissions.  
590 If we instead consider borders roughly bounded by Le Bourget Airport in the north and Paris-Orly in the south, the  
corresponding values are 0.9% and 11%, which are more in line with the findings and adjustments to the ffCO<sub>2</sub> emissions in  
Lian et al. (2023). It is also consistent with the work by Albarus et al. (2024), who observed much lower signal-to-noise ratios  
further away from the Paris city centre. However, even given the borders extending further into the area with a lower ffCO<sub>2</sub>  
signal-to-noise ratio, Paris has a low biogenic challenge score compared to most of our cities (2<sup>nd</sup> quartile). Hence, even cities  
595 with low scores likely require the use of well-calibrated biospheric models, preferably optimized with complementary direct  
flux measurements and observations of correlated tracers and/or isotopes. This is quite likely to be preferred over the strategy  
to using observations only in the dormant season (e.g. Lauvaux et al., 2016), as this comes with the additional uncertainties of  
using temporal profiles to scale the results to the rest of the year (Super et al., 2020; Super et al., 2021).

600 For the "modelling challenge" most of the metrics are related to the complexity of natural and urban topography, which puts  
high demands on models to accurately resolve the airflow. This is the main driver for Zurich's challenge score (3<sup>rd</sup> quartile).  
However, the study by Berchet et al. (2017) conducted in Zurich shows good performance of their model, which they found  
to fulfil the requirements for air pollution modelling at most of the tested sites. Although the requirement for modelling CO<sub>2</sub>  
is higher, this is promising for cities' abilities to overcome this challenge. The challenge for models to accurately represent  
605 nearby point source emissions is also well-established (e.g. Gaudet et al., 2017; Maier et al., 2022; Brunner et al., 2019). This  
challenge is compounded by large emission quantities stemming from these sources, which generally do not have point-source-  
specific temporal profiles. However, hourly emissions are sometimes available, such as for many power plants throughout  
Europe, but most models cannot include them.

610 The "application-specific observational challenge" currently combines metrics related to how well-suited cities are for making  
satellite and radiocarbon observations. The satellite section currently only includes cloud cover, as this is a crucial factor,  
affecting the number of expected samples (e.g. Kuhlmann et al., 2019). However, the relevance of satellite observations to our  
study is debatable, as only a limited number of cities (15) had emission quantities greater than 7.33 MtCO<sub>2</sub> yr<sup>-1</sup> in 2018, which  
is the threshold suggested by Wang et al. (2020) for possible monitoring from space with the CO2M instrument. In the future,  
615 considering separate challenge scores for the different observational methods could be beneficial, allowing cities to evaluate  
their options independently.

For the use of <sup>14</sup>CO<sub>2</sub> observations, the observational challenge is linked to how much contribution is expected from emissions  
from nuclear facilities. As in previous studies (e.g., Maier et al., 2023), we used a flat annual emission rate to simulate this,  
620 but improving the resolution of emission data is a priority at the ICOS Radiocarbon Laboratory. For example, knowing the  
timing of emissions from La Hague, France, would significantly enhance the feasibility of using radiocarbon in many cities  
beyond those closest to it. In 2021, La Hague accounted for 39% of the <sup>14</sup>C in CO<sub>2</sub> emissions from European nuclear facilities



(Storm et al., 2024b), with large quantities released during short periods. Excluding La Hague’s emissions from our analyses, thereby simulating conditions between major emission events, reduces the nuclear masking potential’s 10<sup>th</sup> to 90<sup>th</sup> percentile range from 5-20% to 3-11%. This highlights how our findings can guide and motivate future efforts and underscores the importance of updating our analyses as new data becomes available to the community. In addition, the nuclear challenge also depends on the <sup>14</sup>CO<sub>2</sub> sampling strategy to be established within the city. When coordinated upwind and downwind sampling is employed, it can be assumed that most of the nuclear contribution will be captured in the up-and-downwind samples and is thus intrinsically corrected.

Our focus has been on placing our results within the context of existing urban CO<sub>2</sub> monitoring studies, with particular attention to our three pilot cities. While it was not feasible nor possible to evaluate each individual metric and its true relevance to the challenges, our framework offers a foundation for future discussion and refinement as the research field progresses. Within ICOS Cities, it can support the project vision of developing “blueprints” for monitoring emissions in European cities. We recommend a modular approach for this, enabling cities to match with and adopt strategies from the pilot city that is most similar in ways relevant to the specific challenges. This approach is comparable to that of the “Twinning Learning Program”, part of the European Union’s mission “100 Climate-Neutral and Smart Cities by 2030”, where cities are paired based on shared barriers to achieving climate neutrality. From a pan-European monitoring strategy perspective, it is important to develop blueprints for strategies that are effective across the diverse characteristic signatures found in Europe. To support this, we identified Bratislava and Copenhagen as cities that are among the most distinct from the three cities currently in the ICOS Cities network, making them strong potential candidates for inclusion into the network. This assessment considered all metrics in combination. A modular approach could also be applied here, highlighting cities with high scores in the “biogenic challenge”—a challenge that is relatively minimal for the three pilot cities—as especially suitable candidates. Bratislava would again be among the recommended cities. All in all, there are numerous ways our framework can be used to create analyses like those presented in this study. Adjustments could be as minor as tweaking the weights of the 18 metrics, or as substantial as conducting entirely different analyses based on a new selection of metrics that are readily available for our cities but not used here.

## 5 Data availability

For the datasets used to derive the metrics in this paper, we refer to the cited references. The resulting collection of 18 metrics, as well as several metrics that were excluded from the study, is published along with the notebook tool (Storm et al., 2025a, <https://doi.org/10.18160/P8SV-B99F>). The tool, published as a Jupyter Notebook programmed in Python along with associated Python files, can also be run directly in the Interactive Computing Environment offered by the ICOS Carbon Portal. Individual PDFs, referred to as “mapbooks”, contain maps and analysis results cities; these are published as a collection and can be downloaded for the individual cities (Storm et al., 2025b, <https://doi.org/10.18160/Z66D-05JT>).



## 655 **6 Conclusions**

This study demonstrates a methodology to understand and quantify the differences between cities and what these differences mean from a CO<sub>2</sub> emission monitoring perspective. Our analysis of 96 cities in western Europe, that are analysed based on 18 defined characteristics, is linked to four key CO<sub>2</sub> monitoring challenges. We show how these challenges can be quantified to provide insights into the evolving network of urban observatories in Europe, with a focus on the ICOS Cities pilot cities: Paris, 660 Munich, and Zurich. Their relationships to the other 93 cities are quantified to illustrate: 1) which monitoring challenges may be most significant, 2) which cities are similar and could benefit from knowledge exchange, and 3) which cities are dissimilar and may serve as candidate cities if there is funding to expand the ICOS Cities network.

Overall, our results suggest that Zurich and Munich are relatively easy to monitor, with Zurich facing the greatest challenge in 665 the “modelling challenge” and Munich in the “application-specific observational challenge”. Paris scores similarly to Zurich in the modelling challenge, but also has high scores in the other challenges except for the “biogenic challenge”. Cities similar to Munich are identified across the different challenges, suggesting, for instance, that monitoring strategies used to address the background challenge in Munich may also be effective in for example Linz (Austria). Paris, Munich, and Zurich fall into two out of five clusters when considering all 18 metrics. Copenhagen and Bratislava are highlighted as prominent cities in clusters 670 that are currently not represented by the ICOS Cities network. These could be interesting candidates if an extension to the pilot network is considered.

We have only highlighted a few examples from the results, which represent just a subset of the potential analyses that can be drawn from the framework we have developed. We refer to Sect. 5 for how to access results for specific cities of interest or to 675 conduct new analyses based on a different set of characteristics.

## **7 Author contribution**

IS, UK, AV, and WP designed the study, with SH contributing to the design of the nuclear contribution metrics (Sect. 2.2.5). ISU and TG provided anthropogenic and biogenic CO<sub>2</sub> fluxes, respectively, along with insights regarding their use. IS developed the Jupyter Notebook tool and mapbooks together with CD’O and UK. IS prepared the manuscript, with 680 contributions from all co-authors.

## **8 Competing interests**

The authors declare that they have no conflict of interest.



## 9 Financial support

This work has been supported by the ICOS PAUL project: PAUL, Pilot Applications in Urban Landscapes - Towards integrated  
685 city observatories for greenhouse gases (ICOS Cities), funded by the European Union's Horizon 2020 Research and Innovation  
Programme under grant agreement No 101037319.

## 10 Acknowledgements

The creation of STILT footprints has received funding from the European Union's Horizon 2020 research and innovation  
programme through the ATMO-ACCESS Integrating Activity under grant agreement No 101008004.

690

The biogenic fluxes used in this study were created using resources of the Deutsches Klimarechenzentrum (DKRZ) granted  
by its Scientific Steering Committee (WLA) under project bd1231. The work was financed through the CO2KI project of the  
BMBF (project number FZK50EE2212).

## 11 References

695 Ainsworth, E. A., Yendrek, C. R., Sitch, S., et al.: The effects of tropospheric ozone on net primary productivity and  
implications for climate change, *Annu. Rev. Plant Biol.*, 63, 637–661, <https://doi.org/10.1146/annurev-arplant-042110-103829>, 2012.

Albarus, I., Fleischmann, G., Aigner, P., et al.: From political pledges to quantitative mapping of climate mitigation plans:  
700 Comparison of two European cities, *Carbon Balance Manage.*, 18, 18, <https://doi.org/10.1186/s13021-023-00236-y>, 2023.

Albarus, I., Lauvaux, T., Utard, H., and Denier van der Gon, H.: Bridging Political Pledges and Physical Observations, *Carbon  
Portal, Report*, [https://hdl.handle.net/11676/\\_M6HkIT3Rh983E7HHWNaMs6V](https://hdl.handle.net/11676/_M6HkIT3Rh983E7HHWNaMs6V), 2024.

705 Basu, S., Lehman, S. J., Miller, J. B., Andrews, A. E., Sweeney, C., Gurney, K. R., Xu, X., Southon, J., and Tans, P. P.:  
Estimating US fossil fuel CO<sub>2</sub> emissions from measurements of <sup>14</sup>C in atmospheric CO<sub>2</sub>, *Proc. Natl. Acad. Sci. U.S.A.*, 117,  
13300–13307, <https://doi.org/10.1073/pnas.1919032117>, 2020.

Berchet, A., Zink, K., Oetl, D., Brunner, J., Emmenegger, L., and Brunner, D.: Evaluation of high-resolution GRAMM–  
710 GRAL (v15.12/v14.8) NO<sub>x</sub> simulations over the city of Zürich, Switzerland, *Geosci. Model Dev.*, 10, 3441–3459,  
<https://doi.org/10.5194/gmd-10-3441-2017>, 2017.



715 Berchet, A., Zink, K., Oetl, D., Brunner, J., Emmenegger, L., and Brunner, D.: Evaluation of high-resolution GRAMM–  
GRAL (v15.12/v14.8) NO<sub>x</sub> simulations over the city of Zürich, Switzerland, *Geosci. Model Dev.*, 10, 3441–3459,  
<https://doi.org/10.5194/gmd-10-3441-2017>, 2017.

720 Bréon, F. M., Broquet, G., Puygrenier, V., Chevallier, F., Xueref-Remy, I., Ramonet, M., Dieudonné, E., Lopez, M., Schmidt,  
M., Perrussel, O., and Ciais, P.: An attempt at estimating Paris area CO<sub>2</sub> emissions from atmospheric concentration  
measurements, *Atmos. Chem. Phys.*, 15, 1707–1724, <https://doi.org/10.5194/acp-15-1707-2015>, 2015.

725 Bozhinova, D., van der Molen, M. K., van der Velde, I. R., Krol, M. C., van der Laan, S., Meijer, H. A. J., and Peters, W.:  
Simulating the integrated summertime  $\Delta^{14}\text{CO}_2$  signature from anthropogenic emissions over Western Europe, *Atmos. Chem.*  
*Phys.*, 14, 7273–7290, <https://doi.org/10.5194/acp-14-7273-2014>, 2014.

Brunner, D., Kuhlmann, G., Marshall, J., Clément, V., Fuhrer, O., Broquet, G., Löscher, A., and Meijer, Y.: Accounting for  
the vertical distribution of emissions in atmospheric CO<sub>2</sub> simulations, *Atmos. Chem. Phys.*, 19, 4541–4559,  
<https://doi.org/10.5194/acp-19-4541-2019>, 2019.

730 Buchhorn, M., Smets, B., Bertels, L., De Roo, B., Lesiv, M., Tsendbazar, N.-E., Herold, M., and Fritz, S.: Copernicus Global  
Land Service: Land Cover 100m: Collection 3: Epoch 2019: Globe, Zenodo [data set],  
<https://doi.org/10.5281/zenodo.3939050>, 2020.

735 C40 Cities: C40 Cities, <https://www.c40.org/>, last access: 10 June, 2024.

Denier van der Gon, H., Hendriks, C., Kuenen, J., Segers, A., and Visschedijk, A.: Description of current temporal emission  
patterns and sensitivity of predicted AQ for temporal emission patterns, EU FP7 MACC Deliverable Report D\_D-EMIS\_1, 3,  
2019-07, 2011. Available at: [https://atmosphere.copernicus.eu/sites/default/files/2019-07/MACC\\_TNO\\_del\\_1\\_3\\_v2.pdf](https://atmosphere.copernicus.eu/sites/default/files/2019-07/MACC_TNO_del_1_3_v2.pdf).

740 Dijkstra, L., Poelman, H., and Veneri, P.: The EU-OECD definition of a functional urban area, *OECD Reg. Dev. Work. Pap.*,  
2019, No. 11, <https://doi.org/10.1787/d58cb34d-en>, 2019.

745 European Commission. Communication from the Commission: The European Green Deal (COM/2019/640 final). European  
Commission, 2019. Available at <https://eur-lex.europa.eu/legal-content/EN/TXT/?uri=CELEX%3A52019DC0640>



- European Commission, Directorate-General for Research and Innovation: EU Missions: 100 Climate-Neutral and Smart Cities, Publications Office of the European Union, <https://data.europa.eu/doi/10.2777/85010>, 2024.
- European Environment Agency: EU-DEM, European Environment Agency [data set], <https://sdi.eea.europa.eu/catalogue/srv/api/records/3473589f-0854-4601-919e-2e7dd172ff50>, 2016.
- 750
- Eurostat: GISCO: Geographical Information System of the Commission, Urban Audit 2021 [data set], available at: <https://gisco-services.ec.europa.eu/distribution/v1/urau-2021.html>, accessed on February 27, 2024.
- Gately, C. K., and Hutrya, L. R.: Large uncertainties in urban-scale carbon emissions, *J. Geophys. Res.-Atmos.*, 122, 242–
- 755 260, <https://doi.org/10.1002/2017JD027359>, 2017.
- pyVPRM, GitHub [code], <https://github.com/tglauch/pyVPRM>, last accessed 22 October 2024.
- Global Covenant of Mayors for Climate & Energy: Global Covenant of Mayors Common Reporting Framework v. 7.0, 2023, available at: <https://www.globalcovenantofmayors.org/our-initiatives/data4cities/common-global-reporting-framework/>,
- 760 accessed on June 10, 2024.
- Gaudet, B. J., Lauvaux, T., Deng, A., and Davis, K. J.: Exploration of the impact of nearby sources on urban atmospheric inversions using large eddy simulation, *Elementa-Sci. Anthropol.*, 5, 60, <https://doi.org/10.1525/elementa.247>, 2017.
- 765 Graven, H. D., and Gruber, N.: Continental-scale enrichment of atmospheric  $^{14}\text{CO}_2$  from the nuclear power industry: potential impact on the estimation of fossil fuel-derived  $\text{CO}_2$ , *Atmos. Chem. Phys.*, 11, 12339–12349, <https://doi.org/10.5194/acp-11-12339-2011>, 2011.
- Gurney, K. R., Liang, J., Patarasuk, R., O’Keeffe, D., Huang, J., Hutchins, M., Lauvaux, T., Turnbull, J. C., and Shepson, P.
- 770 B.: Reconciling the differences between a bottom-up and inverse-estimated FFCO<sub>2</sub> emissions estimate in a large US urban area, *Elementa-Sci. Anthropol.*, 5, 44, <https://doi.org/10.1525/elementa.137>, 2017.
- Gurney, K. R., Liang, J., Patarasuk, R., Song, Y., Huang, J., and Roest, G.: Vulcan: High-resolution annual fossil fuel CO<sub>2</sub> emissions in USA, 2010–2015, Version 3, ORNL Distrib. Act. Arch. Cent., <https://doi.org/10.3334/ORNLDAAC/1741>, 2020.
- 775
- Gurney, K. R., Liang, J., Roest, G., et al.: Under-reporting of greenhouse gas emissions in U.S. cities, *Nat. Commun.*, 12, 553, <https://doi.org/10.1038/s41467-020-20871-0>, 2021.



- 780 Hardiman, B. S., Wang, J. A., Hutyra, L. R., Gately, C. K., Getson, J. M., and Friedl, M. A.: Accounting for urban biogenic  
fluxes in regional carbon budgets, *Sci. Total Environ.*, 592, 366–372, <https://doi.org/10.1016/j.scitotenv.2017.03.028>, 2017.
- Havu, M., Kulmala, L., Lee, H. S., Saranko, O., Soininen, J., and Ahongshangbam, J.: CO<sub>2</sub> uptake of urban vegetation in a  
warming Nordic city, *Urban For. Urban Green.*, 94, <https://doi.org/10.1016/j.ufug.2024.128261>, 2024.
- 785 Hersbach, H., Bell, B., Berrisford, P., Biavati, G., Horányi, A., Muñoz Sabater, J., Nicolas, J., Peubey, C., Radu, R., Rozum,  
I., Schepers, D., Simmons, A., Soci, C., Dee, D., and Thépaut, J.-N.: ERA5 Hourly Data on Single Levels from 1940 to Present,  
Copernicus Climate Change Service (C3S) Climate Data Store (CDS) [data set], <https://doi.org/10.24381/cds.adbb2d47>,  
accessed on 12-03-2023, 2023.
- Hsu, A., Tan, J., Ng, Y. M., et al.: Performance determinants show European cities are delivering on climate mitigation, *Nat.*  
790 *Clim. Chang.*, 10, 1015–1022, <https://doi.org/10.1038/s41558-020-0879-9>, 2020.
- ICOS RI, ICOS ETC: Ecosystem Final Quality (L2) Product in ETC-Archive Format - INTERIM Release 2023-2, [data set],  
<https://doi.org/10.18160/JYAR-7YEH>, 2023.
- 795 ICLEI: International Council for Local Environmental Initiative, <https://iclei.org/>, last access: 10 June 2024.
- Jung, M., Henkel, K., Herold, M., and Churkina, G.: Exploiting synergies of global land cover products for carbon cycle  
modeling, *Remote Sens. Environ.*, 101, 534–553, <https://doi.org/10.1016/j.rse.2006.01.020>, 2006.
- 800 Karstens, U.: ICOS Carbon Portal STILT Footprint Tool model set-up description, ICOS RI,  
<https://hdl.handle.net/11676/CXlfZnsBKibuov6SkJ8eIIvX>, 2023.
- Kljun, N., Calanca, P., Rotach, M. W., and Schmid, H. P.: A simple two-dimensional parameterisation for Flux Footprint  
Prediction (FFP), *Geosci. Model Dev.*, 8, 3695–3713, <https://doi.org/10.5194/gmd-8-3695-2015>, 2015.
- 805 Kuenen, J., Dellaert, S., Visschedijk, A., Jalkanen, J.-P., Super, I., and Denier van der Gon, H.: CAMS-REG-v4: a state-of-  
the-art high-resolution European emission inventory for air quality modelling, *Earth Syst. Sci. Data*, 14, 491–515,  
<https://doi.org/10.5194/essd-14-491-2022>, 2022.
- 810 Kuhlmann, G., Broquet, G., Marshall, J., Clément, V., Löscher, A., Meijer, Y., and Brunner, D.: Detectability of CO<sub>2</sub> emission  
plumes of cities and power plants with the Copernicus Anthropogenic CO<sub>2</sub> Monitoring (CO<sub>2</sub>M) mission, *Atmos. Meas. Tech.*,  
12, 6695–6719, <https://doi.org/10.5194/amt-12-6695-2019>, 2019.



815 Lauvaux, T., Schuh, A. E., Uliasz, M., Richardson, S., Miles, N., Andrews, A. E., Sweeney, C., Diaz, L. I., Martins, D., Shepson, P. B., and Davis, K. J.: Constraining the CO<sub>2</sub> budget of the corn belt: exploring uncertainties from the assumptions in a mesoscale inverse system, *Atmos. Chem. Phys.*, 12, 337–354, <https://doi.org/10.5194/acp-12-337-2012>, 2012.

820 Lauvaux, T., Miles, N. L., Deng, A., Richardson, S. J., Cambaliza, M. O., Davis, K. J., Gaudet, B., Gurney, K. R., Huang, J., O’Keefe, D., Song, Y., Karion, A., Oda, T., Patarasuk, R., Razlivanov, I., Sarmiento, D., Shepson, P., Sweeney, C., Turnbull, J., and Wu, K.: High-resolution atmospheric inversion of urban CO<sub>2</sub> emissions during the dormant season of the Indianapolis Flux Experiment (INFLUX), *J. Geophys. Res. Atmos.*, 121, 5213–5236, <https://doi.org/10.1002/2015JD024473>, 2016.

Lauvaux, T., Gurney, K. R., Miles, N. L., Davis, K. J., Richardson, S. J., Deng, A., Nathan, B. J., Oda, T., Wang, J. A., Hutyra, L., and Turnbull, J.: Policy-relevant assessment of urban CO<sub>2</sub> emissions, *Environ. Sci. Technol.*, 54, 10237–10245, <https://doi.org/10.1021/acs.est.0c00343>, 2020.

825

Levin, I., Kromer, B., Schmidt, M., and Sartorius, H.: A novel approach for independent budgeting of fossil fuel CO<sub>2</sub> over Europe by <sup>14</sup>CO<sub>2</sub> observations, *Geophys. Res. Lett.*, 30, 2194, <https://doi.org/10.1029/2003GL018477>, 2003.

830 Levin, I., Karstens, U., Eritt, M., Maier, F., Arnold, S., Rzesanke, D., Hammer, S., Ramonet, M., Vítková, G., Conil, S., Heliasz, M., Kubistin, D., and Lindauer, M.: A dedicated flask sampling strategy developed for Integrated Carbon Observation System (ICOS) stations based on CO<sub>2</sub> and CO measurements and Stochastic Time-Inverted Lagrangian Transport (STILT) footprint modelling, *Atmos. Chem. Phys.*, 20, 11161–11180, <https://doi.org/10.5194/acp-20-11161-2020>, 2020.

835 Lwasa, S., Seto, K. C., Bai, X., Blanco, H., Gurney, K. R., Kılıç, Ş., Lucon, O., Murakami, J., Pan, J., Sharifi, A., Yamagata, Y., and IPCC (2022): Urban systems and other settlements, *Climate Change 2022: Mitigation of Climate Change. Contribution of Working Group III to the Sixth Assessment Report of the Intergovernmental Panel on Climate Change* [P.R. Shukla, J. Skea, R. Slade, A. Al Khourdajie, R. van Diemen, D. McCollum, M. Pathak, S. Some, P. Vyas, R. Fradera, M. Belkacemi, A. Hasija, G. Lisboa, S. Luz, J. Malley, (eds.)], Cambridge University Press, Cambridge, UK and New York, NY, USA, <https://doi.org/10.1017/9781009157926.010>, 2022.

840

Lian, J., Bréon, F.-M., Broquet, G., Lauvaux, T., Zheng, B., Ramonet, M., Xueref-Remy, I., Kotthaus, S., Haeffelin, M., and Ciais, P.: Sensitivity to the sources of uncertainties in the modeling of atmospheric CO<sub>2</sub> concentration within and in the vicinity of Paris, *Atmos. Chem. Phys.*, 21, 10707–10726, <https://doi.org/10.5194/acp-21-10707-2021>, 2021.

845 Lian, J., Lauvaux, T., Utard, H., Bréon, F.-M., Broquet, G., Ramonet, M., Laurent, O., Albarus, I., Chariot, M., Kotthaus, S., Haeffelin, M., Sanchez, O., Perrussel, O., Denier van der Gon, H. A., Dellaert, S. N. C., and Ciais, P.: Can we use atmospheric



- CO<sub>2</sub> measurements to verify emission trends reported by cities? Lessons from a 6-year atmospheric inversion over Paris, *Atmos. Chem. Phys.*, 23, 8823–8835, <https://doi.org/10.5194/acp-23-8823-2023>, 2023.
- 850 Lopez, M., Schmidt, M., Delmotte, M., Colomb, A., Gros, V., Janssen, C., Lehman, S. J., Mondelain, D., Perrussel, O., Ramonet, M., Xueref-Remy, I., and Bousquet, P.: CO, NO<sub>x</sub> and <sup>13</sup>CO<sub>2</sub> as tracers for fossil fuel CO<sub>2</sub>: results from a pilot study in Paris during winter 2010, *Atmos. Chem. Phys.*, 13, 7343–7358, <https://doi.org/10.5194/acp-13-7343-2013>, 2013.
- Mahadevan, P., Wofsy, S. C., Matross, D. M., Xiao, X., Dunn, A. L., Lin, J. C., Gerbig, C., Munger, J. W., Chow, V. Y., and  
855 Gottlieb, E. W.: A satellite-based biosphere parameterization for net ecosystem CO<sub>2</sub> exchange: Vegetation Photosynthesis and Respiration Model (VPRM), *Global Biogeochem. Cycles*, 22, GB2005, <https://doi.org/10.1029/2006GB002735>, 2008.
- Maier, F., Gerbig, C., Levin, I., Super, I., Marshall, J., and Hammer, S.: Effects of point source emission heights in WRF–  
860 STILT: a step towards exploiting nocturnal observations in models, *Geosci. Model Dev.*, 15, 5391–5406, <https://doi.org/10.5194/gmd-15-5391-2022>, 2022.
- Maier, F., Levin, I., Gachkivskyi, M., Rödenbeck, C., and Hammer, S.: Estimating regional fossil fuel CO<sub>2</sub> concentrations from <sup>14</sup>CO<sub>2</sub> observations: challenges and uncertainties, *Philos. Trans. R. Soc. A*, 381, 20220203, <https://doi.org/10.1098/rsta.2022.0203>, 2023.
- 865 Miles, N. L., Davis, K. J., Richardson, S. J., Lauvaux, T., Martins, D. K., Deng, A. J., Balashov, N., Gurney, K. R., Liang, J., Roest, G., Wang, J. A., and Turnbull, J. C.: The influence of near-field fluxes on seasonal CO<sub>2</sub> enhancements: Results from the Indianapolis Flux Experiment (INFLUX), *Carbon Balance Manag.*, 16, 4, <https://doi.org/10.1186/s13021-020-00166-z>, 2021.
- 870 Miller, J. B., Lehman, S. J., Verhulst, K. R., Miller, C. E., Duren, R. M., Yadav, V., et al.: Large and seasonally varying biospheric CO<sub>2</sub> fluxes in the Los Angeles megacity revealed by atmospheric radiocarbon, *Proc. Natl. Acad. Sci. U. S. A.*, 117, 26681–26687, <https://doi.org/10.1073/pnas.2005253117>, 2020.
- 875 Munassar, S., Monteil, G., Scholze, M., Karstens, U., Rödenbeck, C., Koch, F.-T., Totsche, K. U., and Gerbig, C.: Why do inverse models disagree? A case study with two European CO<sub>2</sub> inversions, *Atmos. Chem. Phys.*, 23, 2813–2828, <https://doi.org/10.5194/acp-23-2813-2023>, 2023.



- 880 Nathan, B. J., Lauvaux, T., Turnbull, J. C., Richardson, S. J., Miles, N. L., and Gurney, K. R.: Source sector attribution of CO<sub>2</sub> emissions using an urban CO/CO<sub>2</sub> Bayesian inversion system, *J. Geophys. Res. Atmos.*, 123, 13611–13621, <https://doi.org/10.1029/2018JD029231>, 2018.
- Pastorello, G., Trotta, C., Canfora, E., et al.: The FLUXNET2015 dataset and the ONEFlux processing pipeline for eddy covariance data, *Sci. Data*, 7, 225, <https://doi.org/10.1038/s41597-020-0534-3>, 2020.
- 885 Pesaresi, M., and Politis, P.: GHS-BUILT-H R2023A - GHS building height, derived from AW3D30, SRTM30, and Sentinel2 composite (2018), European Commission, Joint Research Centre (JRC) [data set], <https://doi.org/10.2905/85005901-3A49-48DD-9D19-6261354F56FE>, 2023.
- 890 Pieber, S. M., Tuzson, B., Henne, S., Karstens, U., Gerbig, C., Koch, F.-T., Brunner, D., Steinbacher, M., and Emmenegger, L.: Analysis of regional CO<sub>2</sub> contributions at the high Alpine observatory Jungfraujoch by means of atmospheric transport simulations and δ<sup>13</sup>C, *Atmos. Chem. Phys.*, 22, 10721–10749, <https://doi.org/10.5194/acp-22-10721-2022>, 2022.
- Riley, S. J., DeGloria, S. D., and Elliot, R.: A Terrain Ruggedness Index that quantifies topographic heterogeneity, *Intermountain J. Sci.*, 5, 23–27, 1999.
- 895 Roman, L. A., and Scatena, F. N.: Street tree survival rates: Meta-analysis of previous studies and application to a field survey in Philadelphia, PA, USA, *Urban For. Urban Greening*, 10, 269–274, <https://doi.org/10.1016/j.ufug.2011.05.008>, 2011.
- 900 Sargent, M., Barrera, Y., Nehrkorn, T., Hutyra, L. R., Gately, C. K., Jones, T., McKain, K., Sweeney, C., Hegarty, J., Hardiman, B., Wang, J. A., and Wofsy, S. C.: Anthropogenic and biogenic CO<sub>2</sub> fluxes in the Boston urban region, *Proc. Natl. Acad. Sci. U.S.A.*, 115, 7491–7496, <https://doi.org/10.1073/pnas.1803715115>, 2018.
- 905 Sierk, B., Bézy, J.-L., Löscher, A., and Meijer, Y.: The European CO<sub>2</sub> Monitoring Mission: Observing anthropogenic greenhouse gas emissions from space, *SPIE*, 237–250, <https://doi.org/10.1117/12.2535941>, 2019.
- Smith, I. A., Dearborn, V. K., and Hutyra, L. R.: Live fast, die young: Accelerated growth, mortality, and turnover in street trees, *PLOS ONE*, 14, <https://doi.org/10.1371/journal.pone.0228435>, 2019.
- 910 Stauffer, J., Broquet, G., Bréon, F.-M., Puygrenier, V., Chevallier, F., Xueref-Rémy, I., Dieudonné, E., Lopez, M., Schmidt, M., Ramonet, M., Perrussel, O., Lac, C., Wu, L., and Ciais, P.: The first 1-year-long estimate of the Paris region fossil fuel



- CO<sub>2</sub> emissions based on atmospheric inversion, *Atmos. Chem. Phys.*, 16, 14703–14726, <https://doi.org/10.5194/acp-16-14703-2016>, 2016.
- 915 Storm, I., and Karstens, U.: Radiocarbon nuclear contribution tool, ICOS ERIC - Carbon Portal [data set/code], <https://doi.org/10.18160/GATA-SGZ5>, 2024a.
- Storm, I., Maier, F., Levin, I., Preunkert, S., Karstens, U., and ICOS RI: Annual emission totals of <sup>14</sup>CO<sub>2</sub> from nuclear facilities, [data set], [https://hdl.handle.net/11676/Qa5PvLgEeiXW3IRAfTU5d\\_Oo](https://hdl.handle.net/11676/Qa5PvLgEeiXW3IRAfTU5d_Oo), 2024b.
- 920 Storm, I., Karstens, U., and D'Onofrio, C.: CO<sub>2</sub> Monitoring Challenges Notebook Package, ICOS RI [data set/code], <https://doi.org/10.18160/P8SV-B99F>, 2025a.
- Storm, I., Karstens, U., and D'Onofrio, C.: CO<sub>2</sub> Monitoring Challenges City Mapbooks, ICOS RI [data set],  
925 <https://doi.org/10.18160/Z66D-05JT>, 2025b.
- Storm, I., Karstens, U., D'Onofrio, C., Vermeulen, A., and Peters, W.: A view of the European carbon flux landscape through the lens of the ICOS atmospheric observation network, *Atmos. Chem. Phys.*, 23, 4993–5008, <https://doi.org/10.5194/acp-23-4993-2023>, 2023.
- 930 Super, I., Denier van der Gon, H. A. C., van der Molen, M. K., Sterk, H. A. M., Hensen, A., and Peters, W.: A multi-model approach to monitor emissions of CO<sub>2</sub> and CO from an urban–industrial complex, *Atmos. Chem. Phys.*, 17, 13297–13316, <https://doi.org/10.5194/acp-17-13297-2017>, 2017.
- 935 Super, I., Dellaert, S. N. C., Visschedijk, A. J. H., and Denier van der Gon, H. A. C.: Uncertainty analysis of a European high-resolution emission inventory of CO<sub>2</sub> and CO to support inverse modelling and network design, *Atmos. Chem. Phys.*, 20, 1795–1816, <https://doi.org/10.5194/acp-20-1795-2020>, 2020.
- Super, I., Dellaert, S. N. C., Tokaya, J. P., and Schaap, M.: The impact of temporal variability in prior emissions on the  
940 optimization of urban anthropogenic emissions of CO<sub>2</sub>, CH<sub>4</sub>, and CO using in-situ observations, *Atmos. Environ.*, 11, 100119, <https://doi.org/10.1016/j.aeaoa.2021.100119>, 2021.
- Theobald, D. M., Harrison-Atlas, D., Monahan, W. B., and Albano, C. M.: Ecologically-relevant maps of landforms and physiographic diversity for climate adaptation planning, *PLoS ONE*, 10, e0143619,  
945 <https://doi.org/10.1371/journal.pone.0143619>, 2015.



- Turnbull, J. C., Miller, J. B., Lehman, S. J., et al.: Comparison of  $^{14}\text{CO}_2$ ,  $\text{CO}$ , and  $\text{SF}_6$  as tracers for determination of recently added fossil fuel  $\text{CO}_2$  in the atmosphere and implications for biological  $\text{CO}_2$  exchange, *Geophys. Res. Lett.*, 33, L01817, <https://doi.org/10.1029/2005GL024213>, 2006.
- 950
- Turnbull, J. C., Karion, A., Fischer, M. L., Faloona, I., Guilderson, T., Lehman, S. J., Miller, B. R., Miller, J. B., Montzka, S., Sherwood, T., Saripalli, S., Sweeney, C., and Tans, P. P.: Assessment of fossil fuel carbon dioxide and other anthropogenic trace gas emissions from airborne measurements over Sacramento, California in spring 2009, *Atmos. Chem. Phys.*, 11, 705–721, <https://doi.org/10.5194/acp-11-705-2011>, 2011.
- 955
- Turnbull, J. C., Sweeney, C., Karion, A., Newberger, T., Tans, P., et al.: Towards quantification and source sector identification of fossil fuel  $\text{CO}_2$  emissions from an urban area: Results from the INFLUX experiment, *J. Geophys. Res. Atmos.*, <https://doi.org/10.1002/2014JD022555>, 2015.
- United Nations, Department of Economic and Social Affairs, Population Division (UNDESA): World Urbanization Prospects: The 2018 Revision, Online Edition, United Nations, <https://population.un.org/wup/Publications/>, 2018.
- 960
- Vermote, E.: MODIS/Terra Surface Reflectance 8-Day L3 Global 500m SIN Grid V061 [Data set], NASA EOSDIS Land Processes Distributed Active Archive Center, <https://doi.org/10.5067/MODIS/MOD09A1.061>, 2021.
- 965
- Wang, Y., Broquet, G., Bréon, F.-M., Lespinas, F., Buchwitz, M., Reuter, M., Meijer, Y., Loescher, A., Janssens-Maenhout, G., Zheng, B., and Ciais, P.: PMIF v1.0: assessing the potential of satellite observations to constrain  $\text{CO}_2$  emissions from large cities and point sources over the globe using synthetic data, *Geosci. Model Dev.*, 13, 5813–5831, <https://doi.org/10.5194/gmd-13-5813-2020>, 2020.
- 970
- Winbourne, J. B., Smith, I. A., Stoyanova, H., Kohler, C., Gately, C. K., Logan, B. A., Reblin, J., Reinmann, A., Allen, D. W., and Hutrya, L. R.: Quantification of urban forest and grassland carbon fluxes using field measurements and a satellite-based model in Washington DC/Baltimore area, *J. Geophys. Res. Biogeosci.*, 127, e2021JG006568, 2022.
- World Meteorological Organization: IG3IS Urban Greenhouse Gas Emission Observation and Monitoring Good Research Practice Guidelines (GAW Report No. 275), <https://library.wmo.int/idurl/4/58055>, 2022.
- 975
- Zanaga, D., Van De Kerchove, R., Daems, D., De Keersmaecker, W., Brockmann, C., Kirches, G., Wevers, J., Cartus, O., Santoro, M., Fritz, S., Lesiv, M., Herold, M., Tsendbazar, N.-E., Xu, P., Ramoino, F., and Arino, O.: ESA WorldCover 10 m 2021 v200 (Version v200) [Data set], Zenodo, <https://doi.org/10.5281/zenodo.7254221>, 2022.